

Electronic Supplementary Information

Systematic comparison of racemic and enantiopure multicomponent crystals of phenylsuccinic acid—the role of chirality

Jean Eudes Odounga Odounga^a and Nikoletta B. Báthori^{*a}

^a *Department of Chemistry, Cape Peninsula University of Technology, P.O. Box 652, Cape Town, 8000, South Africa.*

Corresponding author: Nikoletta B. Báthori, E-mail: bathorin@cput.ac.za; Fax: +27 21 460 3854; Tel: +27 21 460 8354

Experimental details		3
Tables		
Table S1	Properties of the racemic and S-phenylsuccinic acid	5
Table S2	Physical properties of coformers	5
Table S3	Crystal data for $[2\text{tBa}^+][\text{COO}^{2-}]$, $[(\text{R/S})\text{-PSA}^-][\text{ANI}^+]$ and $[(\text{S})\text{-PSA}^{2-}] [2\text{ANI}^+]\cdot\text{ANI}$	6
Table S4	Hydrogen bonds in $[2\text{tBa}^+][\text{COO}^{2-}]$, $[(\text{R/S})\text{-PSA}^-][\text{ANI}^+]$ and $[(\text{S})\text{-PSA}^{2-}] [2\text{ANI}^+]\cdot\text{ANI}$	6
Table S5	Crystal data for (R/S)-PSA·2PYR, (R/S)-PSA·2(4PIC) and (R/S)-PSA·2(2,4LUT)	7
Table S6	Hydrogen bonds in (R/S)-PSA·2PYR, (R/S)-PSA·2(4PIC) and (R/S)-PSA·2(2,4LUT)	7
Table S7	Crystal data for (R/S)-PSA·2(3,4LUT), 2(S)-PSA·4(3,4LUT), $[(\text{R/S})\text{-PSA}^{2-}] 2[3,5\text{LUT}^+]\cdot 2(\text{R/S})\text{-PSA}$ and $2[(\text{S})\text{-PSA}^{2-}]4[3,5\text{LUT}^+]\cdot 4(\text{S})\text{-PSA}$	8
Table S8	Hydrogen bonds in (R/S)-PSA·2(3,4LUT), 2(S)-PSA·4(3,4LUT), $[(\text{R/S})\text{-PSA}^{2-}] 2[3,5\text{LUT}^+]\cdot 2(\text{R/S})\text{-PSA}$ and $2[(\text{S})\text{-PSA}^{2-}]4[3,5\text{LUT}^+]\cdot 4(\text{S})\text{-PSA}$	8
Table S9	Crystal data for (R/S)-PSA·PCA	11
Table S10	Hydrogen bonds in (R/S)-PSA·PCA	11
Table S11	Torsion angles and molecular conformations of PSA in MCCs	12
Table S12	Thermoanalytical data for PSA MCCs	14
Table S13	Densities, voids, solvent percentages for PSA MCCs	15
Figures		
Figure S1	$[2\text{tBa}^+][\text{COO}^{2-}]$ crystal structure with labelled atoms in the ASU (a), hydrogen bonds between the ions (b) and crystal packing view down $[100]$.	5
Figure S2	pKa values of PSA and coformers	14
Figure S3	Occurrence of carboxylic acid and pyridine moieties, and their combination in the CSD	15
Figure S4	Occurrence of carboxylate and pyridinium moieties, and their combination in the CSD	18
Figure S5	Occurrence of carboxylic acid and pyridine moieties, and their combination in the CSD (Organic & Inorganic)	19
Figure S6	Occurrence of carboxylate and pyridinium moieties, and their combination in the CSD (Organic & Inorganic)	19
Figure S7	DSC curve of $[2\text{tBa}^+][\text{COO}^{2-}]$ and the starting material	20
Figure S8	TG curve of $[2\text{tBa}^+][\text{COO}^{2-}]$	20
Figure S9	PXRD curve of $[2\text{tBa}^+][\text{COO}^{2-}]$ and the starting material	21
Figure S10	IR curve of $[2\text{tBa}^+][\text{COO}^{2-}]$ and the starting material	21
Figure S11	DSC curve of $[(\text{R/S})\text{-PSA}^-][\text{ANI}^+]$ and the starting material	22
Figure S12	TG curve of $[(\text{R/S})\text{-PSA}^-][\text{ANI}^+]$	22
Figure S13	PXRD curve of $[(\text{R/S})\text{-PSA}^-][\text{ANI}^+]$ and the starting material	23
Figure S14	IR curve of $[(\text{R/S})\text{-PSA}^-][\text{ANI}^+]$ and the starting material	23
Figure S15	DSC curve of $[(\text{S})\text{-PSA}^{2-}] [2\text{ANI}^+]\cdot\text{ANI}$ and the starting material	24
Figure S16	TG curve of $[(\text{S})\text{-PSA}^{2-}] [2\text{ANI}^+]\cdot\text{ANI}$	24
Figure S17	PXRD curve of $[(\text{S})\text{-PSA}^{2-}] [2\text{ANI}^+]\cdot\text{ANI}$ and the starting material	25
Figure S18	IR curve of $[(\text{S})\text{-PSA}^{2-}] [2\text{ANI}^+]\cdot\text{ANI}$ and the starting material	25
Figure S19	DSC curve of (R/S)-PSA·2PYR and the starting material	26
Figure S20	TG curve of (R/S)-PSA·2PYR	26
Figure S21	PXRD curve of (R/S)-PSA·2PYR and the starting material	27
Figure S22	IR curve of (R/S)-PSA·2PYR and the starting material	27
Figure S23	DSC curve of (R/S)-PSA·2(4PIC) and the starting material	28
Figure S24	TG curve of (R/S)-PSA·2(4PIC)	28
Figure S25	PXRD curve of (R/S)-PSA·2(4PIC) and the starting material	29
Figure S26	IR curve of (R/S)-PSA·2(4PIC) and the starting material	29
Figure S27	DSC curve of (R/S)-PSA·2(3,4LUT) and the starting material	30
Figure S28	TG curve of (R/S)-PSA·2(3,4LUT)	30
Figure S29	PXRD curve of (R/S)-PSA·2(3,4LUT) and the starting material	31
Figure S30	IR curve of (R/S)-PSA·2(3,4LUT) and the starting material	31
Figure S31	DSC curve of 2(S)-PSA·4(3,4LUT) and the starting material	32
Figure S32	TG curve of 2(S)-PSA·4(3,4LUT)	32
Figure S33	PXRD curve of 2(S)-PSA·4(3,4LUT) and the starting material	33
Figure S34	IR curve of 2(S)-PSA·4(3,4LUT) and the starting material	33
Figure S35	DSC curve of $[(\text{R/S})\text{-PSA}^{2-}] 2[3,5\text{LUT}^+]\cdot 2(\text{R/S})\text{-PSA}$ and the starting material	34
Figure S36	TG curve of $[(\text{R/S})\text{-PSA}^{2-}] 2[3,5\text{LUT}^+]\cdot 2(\text{R/S})\text{-PSA}$	34

Figure S37	PXRD curve of [(R/S)-PSA ²⁻] 2[3,5LUT ⁺].2(R/S)-PSA and the starting material	35
Figure S38	IR curve of [(R/S)-PSA ²⁻] 2[3,5LUT ⁺].2(R/S)-PSA and the starting material	35
Figure S39	DSC curve of 2[(S)-PSA ²⁻]4[3,5LUT ⁺].4(S)-PSA and the starting material	36
Figure S40	TG curve of 2[(S)-PSA ²⁻]4[3,5LUT ⁺].4(S)-PSA	36
Figure S41	PXRD curve of 2[(S)-PSA ²⁻]4[3,5LUT ⁺].4(S)-PSA and the starting material	37
Figure S42	IR curve of 2[(S)-PSA ²⁻]4[3,5LUT ⁺].4(S)-PSA and the starting material	37
Figure S43	DSC curve of (R/S)-PSA·PCA and the starting materials	38
Figure S44	TG curve of (R/S)-PSA·PCA	38
Figure S45	PXRD curve of (R/S)-PSA·PCA and the starting materials	39
Figure S46	IR curve of (R/S)-PSA·PCA and the starting materials	39

Experimental details

Crystallisations

All materials were purchased from Sigma-Aldrich and were used without further purifications. The multicomponents crystals were synthesized by dissolving the solid acid (R/S-PSA or SPSA) in the liquid bases, while the pharmaceutical cocrystal was synthesized by dissolving the 1:1 mixture of the solid API (pyrazine carboxamide) and the solid acid (rac-PSA or S-PSA) in methanol. The mixtures were gently heated to 40-50°C on a hot plate while stirring for the solutions to be clear. After homogenisation, the solutions were allowed to cool down before filtration through a 0.45µm syringe filter into new vials and left for slow evaporation.

Analytical methods

The thermal behaviour of the obtained crystals was recorded with a Perkin Elmer DSC 6000. Crystals taken from the mother liquor were dried with a filter paper and manually crushed. They were placed into a vented aluminium sample pan. The sample sizes were between 2–5 mg and the temperature range typically 25–350°C was at a heating rate of 10-30°C min⁻¹ depending on sample being analysed. The samples were purged with a stream of nitrogen flowing at 20 ml min⁻¹. Calibration was done using Indium as the reference material. A supplementary DTA instrument was used to run one of the crystal samples from an external laboratory. The sample size was between 2-5 mg and the temperature range was from 30-300°C. TGA was performed on a Pyris 6 thermogravimetric analyzer. Approximately 3 mg samples were added to an alumina crucible per samples analysed. The samples were heated over a typical temperature range of 30 to 400°C at a heating rate of 10°C min⁻¹. The samples were purged with a stream of flowing nitrogen throughout the experiment at 20 ml min⁻¹. A supplementary TGA instrument was used to run one of the crystal samples from an external laboratory on a TA Q500 instrument from 25 to 400 °C at a heating rate of 10°C min⁻¹ with a purge gas of dry nitrogen flowing at 60 ml min⁻¹ for comparison of the percentage mass loss with the expected compound. The crystals were dried on filter paper and placed in an open crucible for thermogravimetric analysis. Fourier transform infrared spectra were collected by using a Perkin Elmer FT-IR spectrometer UATR TWO equipped with a diamond crystal, operating in the range 350 - 4000 cm⁻¹ with a resolution of 4 cm⁻¹ and four scans. A Bruker APEX II DUO X-ray diffractometer using graphite monochromated Mo K α (λ = 0.71073 Å) radiation was used for data collections. The selected crystal was cooled using an Oxford Cryostream 700 with liquid nitrogen at a flow rate of 20 ml min⁻¹. The X-rays were produced at 50 kV and 30 mA using a Bruker K780 generator. The selected monocrystalline piece was mounted on a cryoloop and covered with Paratone N oil to retain crystallinity. The stream of nitrogen gas was set at 20 ml min⁻¹. Cell refinement and data reduction were carried out using SAINT-Plus¹. The X-ray diffraction data were scaled for absorption effects by using SADABS². The systematic absences found in the X-ray data were studied and used to determine the point group through contrast with known space groups. The value of $|E^2-1|$ was also inspected specifically for characteristic centrosymmetric and non-centrosymmetric point groups. The space groups were confirmed using XPREP³. The structure was solved by direct method using the SHELXT⁴ program and

¹ Bruker, SAINT-Plus (including XPREP), Version 7.12, Bruker AXS Inc, Madison, Wisconsin, USA, 2004.

² Sheldrick, G. M., SADABS. University of Göttingen, Germany 1996.

³ Bruker, XPREP, Version 6.14, Bruker AXS Inc, Madison, Wisconsin, USA, 2003.

⁴ Sheldrick, G. M., SHELXT, Acta Cryst. 2015, A71, 3-8.

refined by full-matrix least-squares methods with SHELXL-2016⁴. XPREP was also used to prepare input files which were subsequently used in structure determination using X-Seed⁵. Crystal assemblies, information and other figures were generated using Mercury 3.9⁶ software. The Bruker AXS D2 Phaser X-ray Diffractometer was used for analyses of microcrystalline material. Samples were finely ground and mounted onto a low-background sample holder. A diffractogram was acquired under ambient conditions at a power setting of 40 kV and 20 mA in reflection mode.

Hydrogen treatment: Non-hydrogen atoms were refined anisotropically and the hydrogen atoms bound to carbon atoms were placed at idealized positions and refined as riding atoms. If possible, hydroxyl hydrogen atoms were located in the difference electron density map and refined independently. In other cases, the decision about the protonation state of the COOH group was based on the analysis of the C-O bond lengths. The C-O bond lengths close to 1.3 Å were treated as C-OH groups and hydrogen atoms were added with the appropriate restraints. The length of the complementary C-O bonds that were closer to 1.2 Å were treated as C=O double bonds. If both C-O bond lengths were similar, i.e. resembled delocalisation, the group was treated as a COO⁻. To support the decision based on the C-O bond length, the protonation state of the nitrogen atoms of the coformers were analysed in a similar manner.

Materials

(R/S)-Phenylsuccinic acid and (S)-Phenylsuccinic acid were used. The chemical formula, molar masses and melting points of these weak acids are listed in Table S1. Tert-butylamine (tBa), aniline (ANI), pyridine (PYR), 4-picoline (4PIC), 2,4-Lutidine (2,4LUT), 3,4-lutidine (3,4LUT), 3,5-lutidine (3,5LUT) and pyrazine carboxamide (PCA) were purchased from Sigma-Aldrich and Merck & Co. The chemical formula as well as the molecular mass, boiling and melting point of the amines and the PCA are listed in Table S2. The amines used for this research are derivatives of pyridine and differ by the position and number of the methyl groups on the phenyl ring to study effect of the position of the functional groups on the crystal packing.

[2tBa⁺][COO²⁻]

The [2tBa⁺][COO²⁻] crystallised in the trigonal $R\bar{3}c$ space group (No. 167) with $\frac{1}{3}$ tBa⁺ and $\frac{1}{6}$ COO²⁻ in the asymmetric unit (ASU), (ESI, Fig. S1a). Each oxygen atom hydrogen bonds to two neighbouring tBa⁺ ions via the N3-H1...O5 interaction and its symmetry generated counterparts (Fig. S1b). The hydrophobic and ionic layers are alternating down the [001] direction (Fig. S1c).

Bulk property analysis

In all cases the selected single crystals were representative of the bulk material. This is evident when the PXRD patterns of the bulk are compared to the respective single crystal structures (see Result of bulk property analysis for all MCCs of PSA section on page 20). Crystallisations were repeated with liquid assisted grinding and it was concluded that the grinding resulted the same compound as the solution crystallisation in all cases, with the exception of [(S)-PSA²⁻][2ANI⁺] \cdot ANI (no solid material was obtained from grinding because of solubility limitations). Remaining impurity from the starting material was noted in the compound obtained by grinding when the formation of 2[(S)-PSA²⁻][4[3,5LUT⁺] \cdot 4(S)-PSA was attempted.

⁵ J. Barbour, *J. Supramol. Chem.*, 2001, 1, 189-191.

⁶ Mercury CSD 4.2.0 - New Features for the Visualization and Investigation of Crystal Structures, C. F. Macrae, I. J. Bruno, J. A. Chisholm, P. R. Edgington, P. McCabe, E. Pidcock, L. Rodriguez-Monge, R. Taylor, J. van de Streek and P. A. Wood, *J. Appl. Cryst.*, 41, 466-470, 2008

Table S 1 Properties of the racemic and *S*-phenylsuccinic acid

Host	Formula	Mr (g.mol ⁻¹)	Mp (°C)
(R/S)-PSA	C ₁₀ H ₁₀ O ₄	194.19	165-168
(S)-PSA	C ₁₀ H ₁₀ O ₄	194.19	173-176

Table S 2 Physical properties of coformers

Coformer	Abbreviation	Formula	Mr (g.mol ⁻¹)	Bp (°C)	Mp (°C)
TERT-BUTYLAMINE	tBa	C ₄ H ₁₁ N	73.14	44-46	n/a
ANILINE	ANI	C ₆ H ₇ N	93.13	183-184	n/a
PYRIDINE	PYR	C ₅ H ₅ N	79.10	115-116	n/a
4-PICOLINE	4PIC	C ₆ H ₇ N	93.13	144-145	n/a
2,4-LUTIDINE	2,4LUT	C ₇ H ₉ N	107.15	160-161	n/a
3,4-LUTIDINE	3,4LUT	C ₇ H ₉ N	107.15	163-164	n/a
3,5-LUTIDINE	3,5LUT	C ₇ H ₉ N	107.15	169-170	n/a
PYRAZINE CARBOXAMIDE	PCA	C ₅ H ₅ N ₃ O	123.11	n/a	189

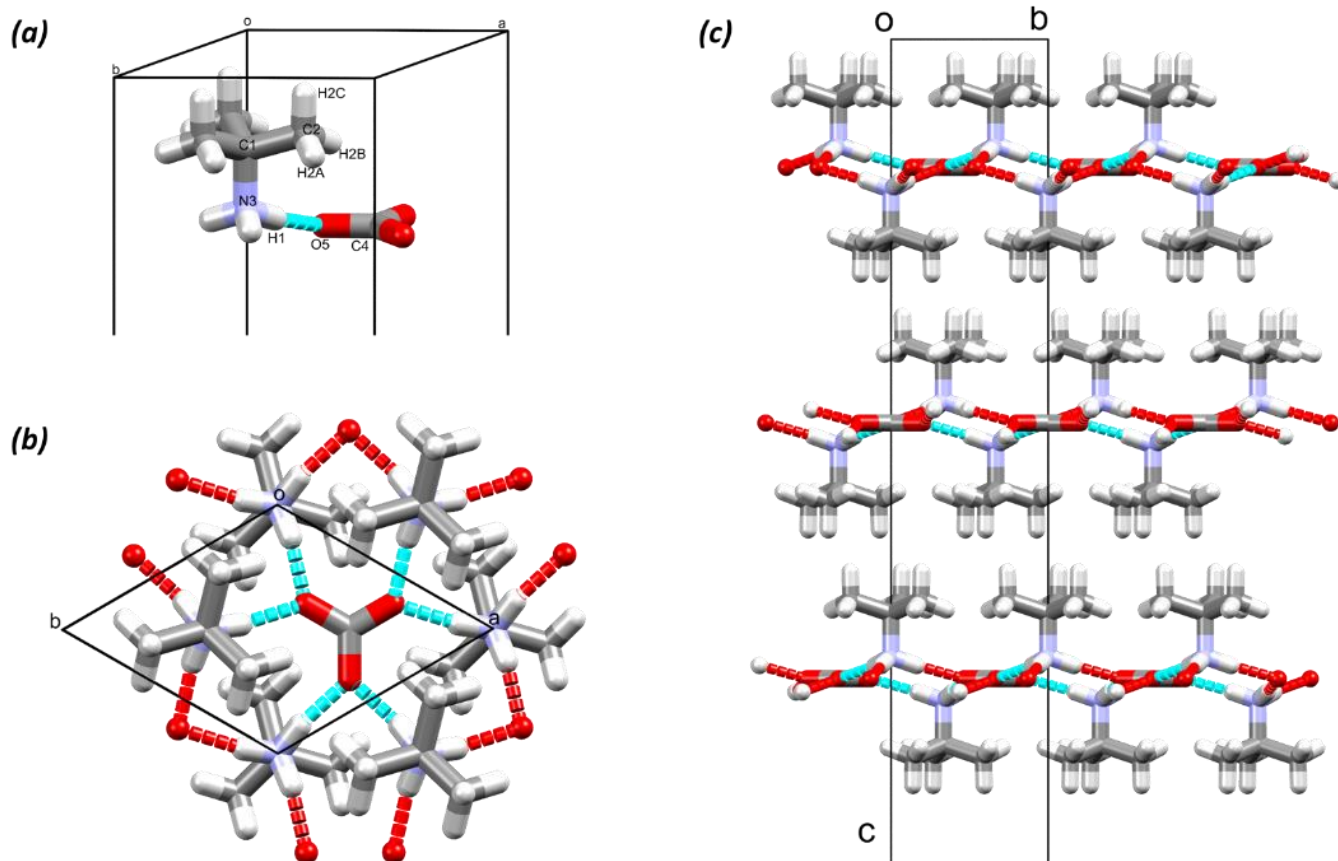


Figure S 1 $[2tBa^+][COO^{2-}]$ crystal structure with labelled atoms in the ASU (a), hydrogen bonds between the ions (b) and crystal packing view down $[100]$ (c)

Table S 3 Crystal data for [2tBa⁺][COO²⁻], [(R/S)-PSA⁻][ANI⁺] and [(S)-PSA²⁻] [2ANI⁺]-ANI

Crystal data			
Compounds	[2tBa ⁺][COO ²⁻]	[(R/S)-PSA ⁻][ANI ⁺]	[(S)-PSA ²⁻][2ANI ⁺]-ANI
Molecular formula	C ₉ H ₂₄ N ₂ O ₃	C ₁₆ H ₁₇ NO ₄	C ₂₈ H ₃₁ N ₃ O ₄
Formula weight (g.mol ⁻¹)	208.30	287.30	473.56
Crystal system	Trigonal	Monoclinic	Orthorhombic
Space group	<i>R</i> 3c (167)	<i>P</i> n(7)	<i>P</i> 2 ₁ (18)
a (Å)	6.3212(9)	9.5310(19)	25.731(5)
b (Å)	6.3212(9)	8.3030(17)	8.2594(17)
c (Å)	53.448(11)	9.885(2)	12.118(2)
α (°)	90	90	90
β (°)	90	111.82(3)	90
γ (°)	120	90	90
V (Å ³)	1849.5(6)	726.2(3)	2575.3(9)
Z	6	2	4
ρ _{calc} /g.cm ⁻³	1.122	1.314	1.221
μ (MoKα) / mm ⁻¹	0.083	0.095	0.082
F (000)	696	304	1008
Crystal size (mm)	0.07 × 0.38 × 0.40	0.04 × 0.240 × 0.300	0.093 × 0.328 × 0.334
Temperature (K)	173(2)	173(2)	173(2)
Radiation [Å]	MoKα (0.71073 Å)	MoKα (0.71073 Å)	MoKα (0.71073 Å)
Theta min-max [°]	2.286, 28.417	2.453, 28.389	1.583, 27.175
Dataset	-8:7, -8:8, -70:70	-12:12, -11:11, -13:13	-33:32, -10:10, -15:15
Final R indices [I > 2.0 (I)]	R ₁ = 0.0331, wR ₂ = 0.0922	R ₁ = 0.0392, wR ₂ = 0.0810	R ₁ = 0.0415, wR ₂ = 0.0996
R indices (all data)	R ₁ = 0.0359, wR ₂ = 0.0946	R ₁ = 0.0500, wR ₂ = 0.0862	R ₁ = 0.0473, wR ₂ = 0.1028
Tot., uniq.data, R (int)	4739, 484, 0.0280	10213, 3039, 0.0316	28838, 5209, 0.0375
N _{ref} , N _{par}	528, 26	3608, 206	5734, 394
S	1.118	0.992	1.068
Max. ans av. Shift/error	0.000, 0.000	0.000, 0.000	0.000, 0.000
Min. and max. resd. Dens (Å ³)	-0.135, 0.287	-0.179, 0.152	-0.223, 0.177

Table S 4 Hydrogen bonds in [2tBa⁺][COO²⁻], [(R/S)-PSA⁻][ANI⁺] and [(S)-PSA²⁻] [2ANI⁺]-ANI

D-H...A	d(D-H) (Å)	d(H...A) (Å)	d(D...A) (Å)	D-H...A (°)	Symmetry operator
[2tBa ⁺][COO ²⁻]					
N3-H1...O5	0.95	1.79	2.730	170.0	
[(R/S)-PSA ⁻][ANI ⁺]					
N15-H15A...O10	1.02	1.67	2.675	168.5	
N15-H15B...O13	0.87	2.36	2.937	124.2	x, y, z+1
N15-H15B...O14	0.87	2.34	2.937	126.1	x-1/2, -y+1, z+1/2
N15-H15C...O11	0.94	1.77	2.714	177.4	x+1/2, -y+1, z+1/2
O14-H14...O11	0.91	1.61	2.523	173.5	x+1/2, -y+1, z-1/2
[(S)-PSA ²⁻] [2ANI ⁺]-ANI					
C17-H17...O13	0.95	2.50	3.265	138.1	
N15-H15A...O13	0.94	2.51	3.024	114.5	
N15-H15A...O14	0.94	1.81	2.721	163.5	
N15-H15B...O11	0.93	1.85	2.743	160.4	x, y+1, z
N22-H22C...O10	0.95	1.79	2.736	174.0	x, y+1, z
N22-H22C...O11	0.95	2.55	3.083	116.0	x, y+1, z
N22-H22A...O13	0.91	1.78	2.684	174.4	
N22-H22B...O10	0.95	1.78	2.723	175.8	-x+1/2, y+1/2, -z
N29-H29A...O11	0.87	2.22	3.089	175.4	
N15-H15C...O14	0.94	1.77	2.709	176.0	-x+1/2, y+1/2, -z+1
C17-H17...O13	0.95	2.50	3.265	138.1	

Table S 5 Crystal data for (R/S)-PSA·2PYR, (R/S)-PSA·2(4PIC) and (R/S)-PSA·2(2,4LUT)

Crystal data			
Compounds	(R/S)-PSA·2PYR	(R/S)-PSA·2(4PIC)	(R/S)-PSA·2(2,4LUT)
Molecular formula	C ₂₀ H ₂₀ N ₂ O ₄	C ₂₂ H ₂₄ N ₂ O ₄	C ₂₄ H ₂₈ N ₂ O ₄
Formula weight (g.mol ⁻¹)	352.38	380.43	408.48
Crystal system	Triclinic	Monoclinic	Monoclinic
Space group	<i>P</i> $\bar{1}$ (2)	<i>P</i> 2 ₁ /c (14)	<i>P</i> 2 ₁ /c (14)
a (Å)	5.6697(4)	22.906(5)	11.773(2)
b (Å)	10.5672(6)	5.7441(11)	8.4930(17)
c (Å)	15.5754(10)	15.376(3)	22.318(5)
α (°)	109.3480(10)	90	90
β (°)	96.6060(10)	100.98(3)	96.22(3)
γ (°)	91.6060(10)	90	90
V (Å ³)	872.44(10)	1986.1(7)	2218.4(8)
Z	2	4	4
$\rho_{\text{calc}}/\text{g.cm}^{-3}$	1.341	1.272	1.223
μ (MoK α) / mm ⁻¹	0.094	0.088	0.083
F (000)	372	808	872
Crystal size (mm)	0.010×0.010×0.010	0.080×0.110×0.210	0.180×0.380×0.570
Temperature (K)	173(2)	173(2)	173(2)
Radiation [Å]	MoK α (0.71073 Å)	MoK α (0.71073 Å)	MoK α (0.71073 Å)
Theta min-max [°]	1.398, 27.532	1.811, 27.131	1.740, 28.452
Dataset	-7:7, -13:13, -20:20	-29:29, -7:3, -19:19	-15:15, -11:11, -28:29
Final R indices [I > 2.0 (I)]	R ₁ =0.0359, wR ₂ =0.0885	R ₁ =0.0782, wR ₂ =0.1954	R ₁ =0.0545, wR ₂ =0.1303
R indices (all data)	R ₁ =0.0389, wR ₂ =0.0907	R ₁ =0.1345, wR ₂ =0.2287	R ₁ =0.0822, wR ₂ =0.1464
Tot., uniq.data, R (int)	23333, 3681, 0.0223	11159, 2529, 0.0316	25976, 3832, 0.0242
N _{ref} , N _{par}	4011, 243	4367, 278	5492, 353
S	1.059	1.035	1.025
Max. ans av. Shift/error	0.001, 0.000	0.000, 0.000	0.000, 0.000
Min. and max. resd. Dens (Å ⁻³)	-0.135, 0.287	-0.283, 0.473	-0.270, 0.256

Table S 6 Hydrogen bonds in (R/S)-PSA·2PYR, (R/S)-PSA·2(4PIC) and (R/S)-PSA·2(2,4LUT)

D-H...A	d(D-H) (Å)	d(H...A) (Å)	d(D...A) (Å)	D-H...A (°)	Symmetry operator
(R/S)-PSA·2PYR					
C8-H8A...O11	0.99	2.55	3.356	138.7	-x+2, -y+2, -z+1
O11-H11...N15	0.95	1.68	2.625	174.4	
O14-H14...N21	0.91	1.80	2.700	174.6	
C17-H17...O10	0.95	2.53	3.427	158.6	-x+1, -y+1, -z+1
C22-H22...O13	0.95	2.66	3.308	126.1	
(R/S)-PSA·2(4PIC)					
C23-H23...O11B	0.84	2.43	2.974	123.5	
O11Aa-H14A...N22	0.84	1.77	2.597	166.5	
O14Aa-H14A...N15	0.84	1.87	2.704	177.0	
O11Bb-H11B...N22	0.84	2.33	2.938	129.2	
(R/S)-PSA·2(2,4LUT)					
O11-H11...N23	1.03	1.59	2.610	168.2	
O14-H14...N15	1.03	1.56	2.587	174.2	
C19-H19...O10	0.95	2.50	3.379	154.3	x+1, y, z
C20-H20...O13	0.95	2.64	3.305	127.6	
C27d-H27d...O13	0.95	2.53	3.463	167.3	x+1, y, z

Table S 7 Crystal data for (R/S)-PSA·2(3,4LUT), 2(S)-PSA·4(3,4LUT), [(R/S)-PSA²⁺] 2[3,5LUT⁺]-2(R/S)-PSA and 2[(S)-PSA²⁺]4[3,5LUT⁺]-4(S)-PSA

Crystal data				
Compounds	(R/S)-PSA· 2(3,4LUT)	2(S)-PSA· 4(3,4LUT)	[(R/S)-PSA ²⁺] 2[3,5LUT ⁺]-2(R/S)-PSA	2[(S)-PSA ²⁺] 4[3,5LUT ⁺]-4(S)-PSA
Molecular formula	C ₂₄ H ₂₈ N ₂ O ₄	C ₂₈ H ₂₈ N ₂ O ₄	C ₂₄ H ₂₈ N ₂ O ₄	C ₈₈ H ₉₆ N ₄ O ₂₄
Formula weight (g.mol ⁻¹)	408.48	408.48	408.48	1593.68
Crystal system	Triclinic	Triclinic	Monoclinic	Triclinic
Space group	<i>P</i> $\bar{1}$ (2)	<i>P</i> 1 (1)	<i>P</i> 2 ₁ /c (14)	<i>P</i> 1 (1)
a (Å)	7.0626(14)	7.1918(14)	12.222(2)	8.3469(17)
b (Å)	8.7704(18)	8.7570(18)	14.926(3)	12.268(3)
c (Å)	18.630(4)	18.766(4)	22.984(5)	20.595(4)
α (°)	90.98(3)	89.75(3)	90	84.66(3)
β (°)	100.42(3)	79.83(3)	103.42(3)	86.58(3)
γ (°)	107.25(3)	72.07(3)	90	76.63(3)
V (Å ³)	1080.8(4)	1105.2(4)	4078.4(15)	2041.2(8)
Z	2	2	4	1
$\rho_{\text{calc}}/\text{g.cm}^{-3}$	1.255	1.227	1.298	1.296
μ (MoK α) / mm ⁻¹	0.086	0.084	0.095	0.095
F (000)	436	436	1688	844
Crystal size (mm)	0.140 × 0.220 × 0.480	0.100 × 0.100 × 0.100	0.100 × 0.200 × 0.240	0.200 × 0.240 × 0.500
Temperature (K)	173(2)	173(2)	173(2)	173(2)
Radiation [Å]	MoK α (0.71073 Å)	MoK α (0.71073 Å)	MoK α (0.71073 Å)	MoK α (0.71073 Å)
Theta min-max [°]	2.229, 28.450	4.015, 26.707	1.640, 27.610	1.712, 28.361
Dataset	-9:9, -11:10, -24:24	-9:9, -11:11, -23:23	-14:15, -19:19, -29:29	-11:11, -16:16, -27:26
Fin. R ind. [I > 2.0 (I)]	R ₁ = 0.0513, wR ₂ = 0.1213	R ₁ = 0.0647, wR ₂ = 0.1511	R ₁ = 0.0696, wR ₂ = 0.1655	R ₁ = 0.0768, wR ₂ = 0.1977
R indices (all data)	R ₁ = 0.0683, wR ₂ = 0.1313	R ₁ = 0.1152, wR ₂ = 0.1786	R ₁ = 0.1101, wR ₂ = 0.1906	R ₁ = 0.1012, wR ₂ = 0.2177
Tot., uniq.data, R (int)	12233, 4166, 0.0265	9225, 5940, 0.075	51410, 6132, 0.0506	46913, 14901, 0.0269
N _{ref} , N _{par}	5423, 284	9225, 546	9432, 609	19773, 1062
S	1.057	1.023	1.030	1.019
Max. ans av. Shift/error	0.000, 0.000	0.000, 0.000	0.000, 0.000	0.000, 0.000
Min. and max. resd. Dens (Å ³)	-0.277, 0.535	-0.338, 0.428	-0.432, 0.933	-0.503, 0.725

Table S 8 Hydrogen bonds in (R/S)-PSA·2(3,4LUT), 2(S)-PSA·4(3,4LUT), [(R/S)-PSA²⁺] 2[3,5LUT⁺]-2(R/S)-PSA and 2[(S)-PSA²⁺]4[3,5LUT⁺]-4(S)-PSA

D-H...A	d(D-H) (Å)	d(H...A) (Å)	d(D...A) (Å)	D-H...A (°)	Symmetry operator
(R/S)-PSA·2(3,4LUT)					
N15-H15...O10	0.92	2.58	3.192	123.9	
N15-H15...O11	0.92	1.83	2.756	176.0	
C16-H16...O10	0.95	2.50	3.150	125.3	
C16-H16...O10Y	0.95	2.26	3.148	155.8	x-1, y, z
C20-H20...O13Y	0.95	2.35	3.204	148.7	
N23-H23...O14	0.92	2.60	3.210	124.3	
N23-H23...O14	0.92	1.80	2.722	179.3	
C24-H24...O10X	0.95	2.31	3.143	146.4	-x, y-1/2, -z+1/2
C28-H28...O13	0.95	2.46	3.132	127.3	
C28-H28...O13X	0.95	2.39	3.267	152.5	-x+1, y-1/2, -z+1/2
C1A-H1A...O14Y	1.00	2.51	3.342	153.8	

D-H...A	d(D-H) (Å)	d(H...A) (Å)	d(D...A) (Å)	D-H...A (°)	Symmetry operator
C8A-H8A1...O11X	0.99	2.43	3.342	152.6	-x, y-1/2, -z+1/2
C1B-H1B...O11X	1.00	2.34	3.292	158.5	-x, y-1/2, -z+1/2
C8B-H8B1...O14Y	0.99	2.48	3.428	160.6	
O14Y-H14Y...O11	0.87	1.73	2.586	170.7	
O14X-H14X...O13	0.91	1.69	2.593	176.9	-x+1, y+1/2, -z+1/2
O11Y-H11Y...O10	0.89	1.73	2.611	171.3	x+1, y, z
O11X-H11X...O14	0.98	1.62	2.600	174.4	-x, y+1/2, -z+1/2
2(S)-PSA·4(3,4LUT)					
C1A-H1A...O11X	1.00	2.41	3.356	157.6	
C8A-H8B...O11Y	0.99	2.46	3.246	135.9	x, y-1, z
N15A-H15A...O13A	0.88	1.82	2.692	173.3	
N15A-H15A...O14A	0.88	2.62	3.208	124.7	
C16A-H16A...O10Y	0.95	2.38	3.238	149.5	x, y-1, z
C20A-H20A...O14A	0.95	2.54	3.180	125.0	
C20A-H20A...O13Y	0.95	2.38	3.235	149.4	
N23A-H23A...O14A	0.88	1.85	2.717	170.2	
C24A-H24A...O10A	0.95	2.51	3.168	126.3	
C24A-H24A...O13X	0.95	2.34	3.212	153.0	x, y-1, z
C28A-H28A...O10X	0.95	2.39	3.232	147.9	
N15B-H15B...O10X	1.10	1.56	2.631	165.1	
C16B-H16B...O10Z	0.95	2.33	3.194	150.3	
C20B-H20B...O13Z	0.95	2.31	3.183	155.7	x, y-1, z
N23B-H23B...O11B	0.76	1.92	2.667	171.8	
C24B-H24B...O10W	0.95	2.31	3.209	158.7	
C28B-H28B...O13W	0.95	2.22	3.059	146.5	x, y-1, z
O11W-H11W...O10B	0.84	1.82	2.656	176.8	
O14W-H14W...O11B	0.84	1.82	2.654	173.6	x, y+1, z
O11X-H11X...O11A	0.84	1.72	2.558	174.6	
O14X-H11X...O10A	0.84	1.78	2.612	170.1	x, y+1, z
O11Y-H11Y...O13A	0.84	1.74	2.573	174.4	x, y+1, z
O14Y-H11Y...O14A	0.84	1.73	2.566	174.0	
O11Z-H11Z...O13B	0.84	1.79	2.611	165.5	
O14Z-H14Z...O14B	0.84	1.88	2.709	170.2	x, y+1, z
[(R/S)-PSA²⁻] 2[3,5LUT⁺]·2(R/S)-PSA					
N15-H15...O10	0.92	2.58	3.192	123.9	
N15-H15...O11	0.92	1.83	2.756	176.0	
C16-H16...O10	0.95	2.50	3.150	125.3	
C16-H16...O10Y	0.95	2.26	3.148	155.8	x-1, y, z
C20-H20...O13Y	0.95	2.35	3.204	148.7	
N23-H23...O13	0.92	2.60	3.210	124.3	
N23-H23...O14	0.92	1.80	2.722	179.3	
C24-H24...O10X	0.95	2.31	3.143	146.4	
C28-H28...O13	0.95	2.46	3.132	127.3	
C28-H28...O13X	0.95	2.39	3.267	152.5	x+1, y, z
C1A-H1A...O14Y	1.00	2.51	3.342	153.8	
C8A-H8A1...O11X	0.99	2.43	3.342	152.6	
C1B-H1B...O11X	1.00	2.34	3.292	158.5	
C8B-H8B...O14Y	0.99	2.48	3.428	160.6	
O14Y-H14Y...O11	0.87	1.73	2.586	170.7	
O14X-H14X...O13	0.91	1.69	2.593	176.9	x-1, y, z
O11Y-H11Y...O10	0.89	1.73	2.611	171.3	x+1, y, z
O11X-H11X...O14	0.98	1.62	2.600	174.4	

D-H...A	d(D-H) (Å)	d(H...A) (Å)	d(D...A) (Å)	D-H...A (°)	Symmetry operator
2[(S)-PSA²⁻]4[3,5LUT⁺]·4(S)-PSA					
C1A-H1A...O11X	1.00	2.41	3.356	157.6	x, y+1, z
C8A-H8B...O11Y	0.99	2.46	3.246	135.9	x, y-1, z
N15A-H15A...O13A	0.88	1.82	2.692	173.3	
N15A-H15A...O14A	0.88	2.62	3.208	124.7	
C16A-H16A...O10Y	0.95	2.38	3.238	149.5	x, y-1, z
C20A-H20A...O14A	0.95	2.54	3.180	125.0	
C20A-H20A...O13Y	0.95	2.38	3.235	149.4	
N23A-H23A...O11A	0.88	1.85	2.717	170.2	
C24A-H24A...O10A	0.95	2.51	3.168	126.3	
C24A-H24A...O13X	0.95	2.34	3.212	153.0	
C28A-H28A...O10X	0.95	2.39	3.231	147.9	x, y+1, z
N15B-H15B...O13B	1.10	1.56	2.631	165.1	
C16B-H16B...O10Z	0.95	2.33	3.194	150.3	x, y+1, z
C20B-H20B...O13Z	0.95	2.31	3.183	155.7	
N23B-H23B...O11B	0.76	1.92	2.667	171.8	
C24B-H24B...O10W	0.95	2.31	3.209	158.7	
C28B-H28B...O13W	0.95	2.22	3.059	146.5	x, y-1, z
O11W-H11W...O10B	0.84	1.82	2.656	176.8	
O14W-H14W...O11B	0.84	1.82	2.654	173.6	x, y+1, z
O11X-H11X...O11A	0.84	1.72	2.558	174.6	x, y-1, z
O14X-H11X...O10A	0.84	1.78	2.612	170.1	
O11Y-H11Y...O13A	0.84	1.74	2.573	174.4	x, y+1, z
O14Y-H11Y...O14A	0.84	1.73	2.566	174.0	
O11Z-H11Z...O13B	0.84	1.79	2.611	165.5	x, y-1, z
O14Z-H14Z...O14B	0.84	1.88	2.709	170.2	

Table S 9 Crystal data for (R/S)-PSA•PCA

Crystal data	
Compounds	(R/S)-PSA•PCA
Molecular formula	C ₁₅ H ₁₅ N ₃ O ₅
Formula weight (g.mol ⁻¹)	317.30
Crystal system	Triclinic
Space group	<i>P</i> $\bar{1}$ (2)
a (Å)	5.7726(12)
b (Å)	7.9815(16)
c (Å)	16.594(3)
α (°)	99.36(3)
β (°)	99.28(3)
γ (°)	97.44(3)
V (Å ³)	734.9(3)
Z	2
ρ_{calc} / g.cm ⁻³	1.434
μ (MoK α) / mm ⁻¹	0.110
F (000)	332
Crystal size (mm)	0.040 × 0.220 × 0.900
Temperature (K)	173(2)
Radiation [Å]	MoK α (0.71073 Å)
Theta min-max [°]	1.266, 28.353
Dataset	-7:7, -10:10, -22:22
Final R indices [I > 2.0 (I)]	R ₁ = 0.0403, wR ₂ = 0.0898
R indices (all data)	R ₁ = 0.0553, wR ₂ = 0.0971
Tot., uniq.data, R (int)	19165, 2858, 0.0416
N _{ref} , N _{par}	3666, 224
S	1.040
Max. ans av. Shift/error	0.001, 0.000
Min. and max. resd. Dens (Å ⁻³)	-0.210, 0.274

Table S 10 Hydrogen bonds in (R/S)-PSA•PCA

D-H...A	d(D-H) (Å)	d(H...A) (Å)	d(D...A) (Å)	D-H...A (°)	Symmetry operator
N17-H17A...O13	0.89	2.08	2.949	163.8	
O14-H14...O15	0.93	1.70	2.619	168.3	
O11-H11...O10	0.91	1.74	2.653	176.0	-x+1, -y+2, -z+1
C20-H20...N22	0.95	2.57	3.418	149.4	x+1, y, z
C23-H23...N19	0.95	2.57	3.419	148.8	x-1, y, z

Table S 11 Torsion angles and molecular conformations of PSA in MCCs

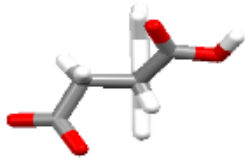
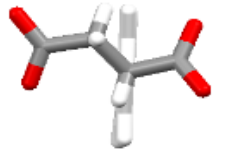
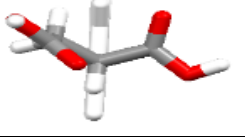
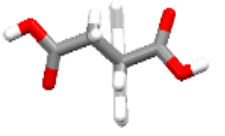
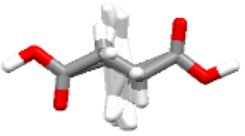
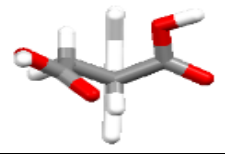
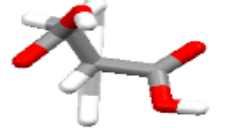
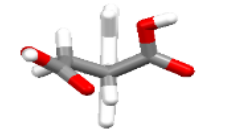
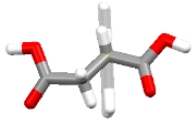
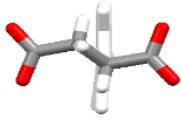
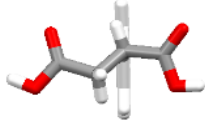
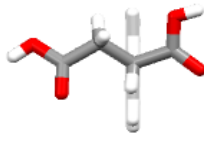
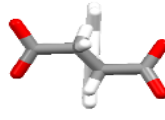
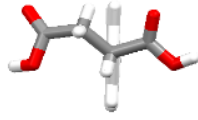
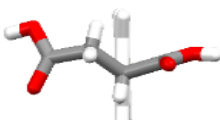

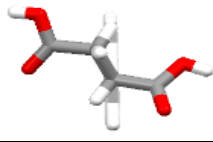

Crystal	$\tau_1(^{\circ})$	$\tau_2(^{\circ})$	$\tau_3(^{\circ})$	Conformation
[(R/S)-PSA \cdot][ANI $^+$]	-64.15	81.82	-130.86	
[(S)-PSA $^{2-}$][2ANI $^+$] \cdot ANI	-105.83	56.68	-160.12	
(R/S)-PSA \cdot 2PYR	-85.26	176.14	-6.65	
(R/S)-PSA \cdot 2(4PIC)	-98.46	65.87	-159.22	
(R/S)-PSA \cdot 2(2,4LUT)	-93.00	111.36	-11.73	
(R/S)-PSA \cdot 2(3,4LUT)	-73.40	169.02	-6.36	
2(S-PSA) \cdot 4(3,4LUT)	-113.11	165.80	-59.68	
	-75.46	171.77	-10.97	

Table S 11 Torsion angles and molecular conformations of PSA in MCCs (cont.)

Crystal	$\tau_1(^{\circ})$	$\tau_2(^{\circ})$	$\tau_3(^{\circ})$	Conformation
[(R/S)-PSA ²⁻] ₂ [3,5LUT ⁺] ₂ ·2(R/S)-PSA	-99.27	-49.03	-42.52	
	-93.93	60.12	-138.99	
	-71.72	-70.57	-31.28	
2[(S)-PSA ²⁻] ₄ [3,5LUT ⁺] ₄ ·4 (S)-PSA	-78.14	70.06	-140.60	
	-117.66	76.08	164.75	
	-71.37	46.24	-130.48	
	-175.88	47.43	-117.61	
	-76.84	61.30	-140.35	
	-127.54	64.23	154.65	
(R/S)-PSA·PCA	-74.06	173.47	-18.10	

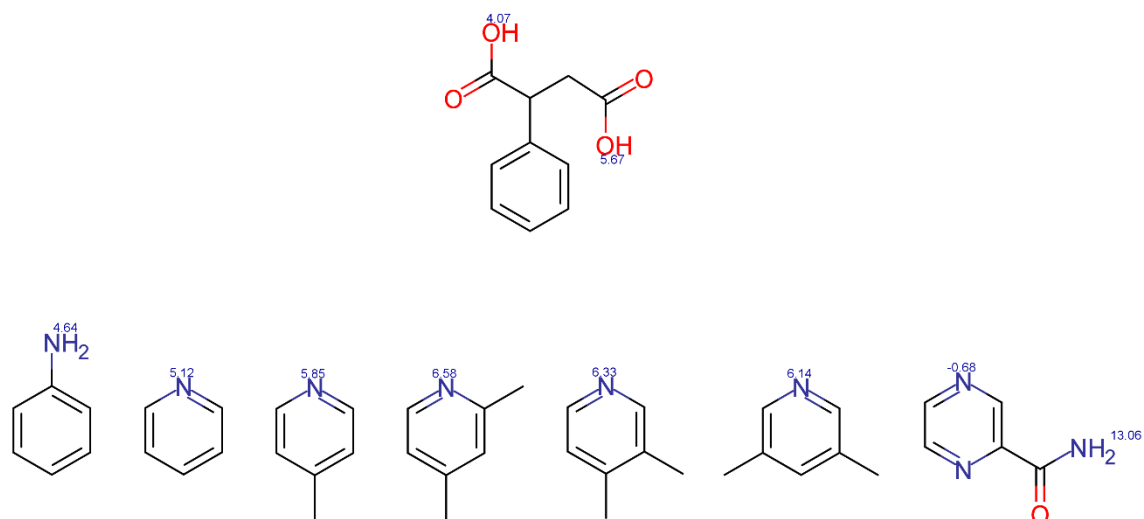


Figure S 2 pK_a values of PSA and coformers

Table S 12 Thermoanalytical data for PSA MCCs

Acid	Coformer	TGA					DSC			
		% DECOMPOSITION					MELTING POINT			
		Measured %	Theoretical %	Difference %	H:G ratio		Onset °C	Peak °C	ΔH J/g	ΔT °C
(R/S)-PSA	-	n/a	n/a	n/a	n/a	n/a	170.15	171.97	146.37	n/a
(S)-PSA	-	n/a	n/a	n/a	n/a	n/a	172.05	177.54	140.15	n/a
PCA	-	n/a	n/a	n/a	n/a	n/a	189.09	191.34	194.54	n/a
(R/S)-PSA	ANI	30.84	32.41	-1.57	1:1	1:1	135.28	137.79	135.66	34.87
(S)-PSA	ANI	48.01	59.00	-10.99	1:2.4	1:3	61.00	63.55	108.30	111.05
(R/S)-PSA	PYR	34.01	44.89	-10.88	1:1.5	1:2	62.17	70.07	97.13	107.98
(R/S)-PSA	4PIC	20.95	48.96	-28.01	1:0.9	1:2	65.72	69.76	92.76	106.33
(R/S)-PSA	3,4LUT	30.61	59.07	-28.46	1:1	1:2	84.99	88.32	146.95	50.29
(S)-PSA	3,4LUT	36.08	68.82	-32.74	2:2.1	2:4	55.46	63.46	80.25	116.59
(R/S)-PSA	3,5LUT	97.32	62.34	n/a	n/a	3:2	134.76	138.78	110.21	35.39
(S)-PSA	3,5LUT	95.51	76.80	n/a	n/a	6:4	97.12	103.19	71.79	74.93
(R/S)-PSA	PCA	97.21	55.91	n/a	n/a	1:2	125.27	130.21	109.97	44.88

*Thermoanalytical results for (R/S)-PSA·2,4LUT were not performed due to scarcity of sample.

* $\Delta T = T_{\text{onset, acid}} - T_{\text{onset, MCC}}$

Table S 13 Densities, voids, solvent percentages for PSA MCCs

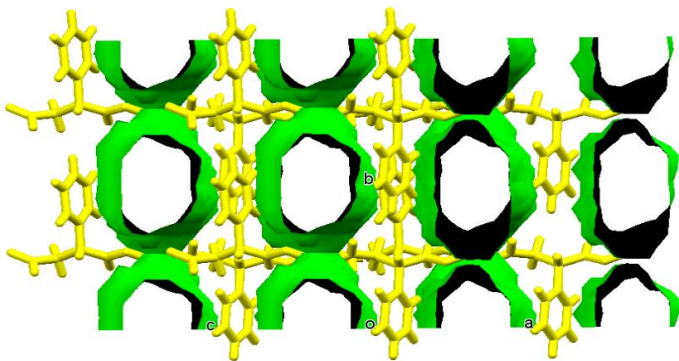
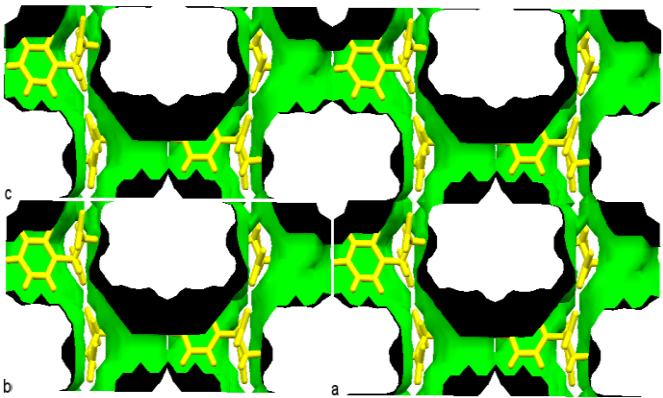
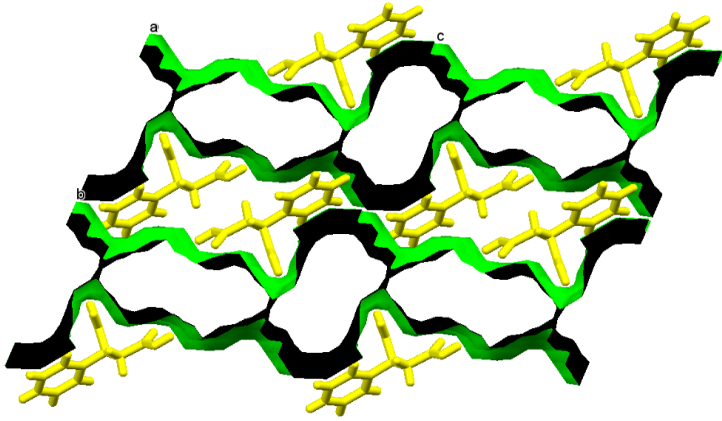
Crystal	Density	%Base	H:G ratio	Type
[(R/S)-PSA⁻][ANI⁺]	1.314 g.cm ⁻³	36.5%	1:1	Tubulate
				
[(S)-PSA²⁻][2ANI⁺·ANI]	1.221 g.cm ⁻³	63.3%	1:3	Tubulate
				
(R/S)-PSA·2PYR	1.341 g.cm ⁻³	44.6%	1:2	Intercalate
				

Table S 14 Densities, voids, solvent percentages for PSA MCCs (cont.)

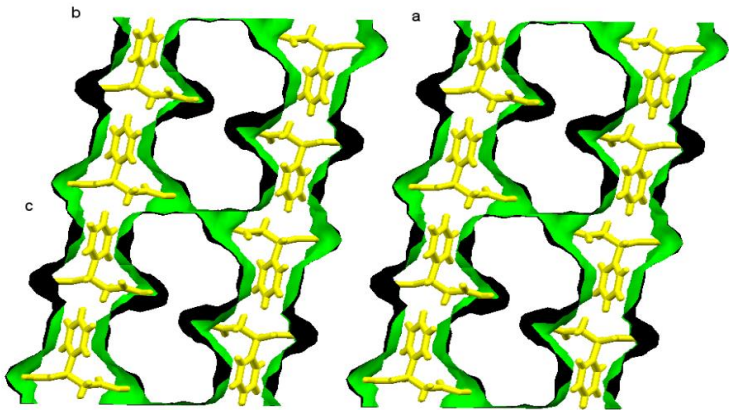
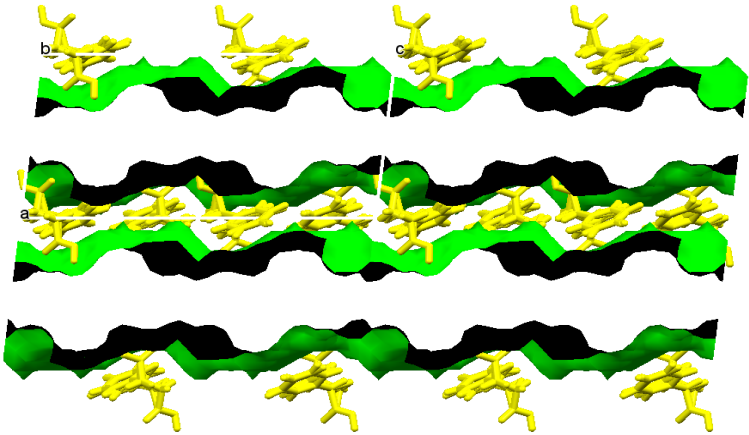
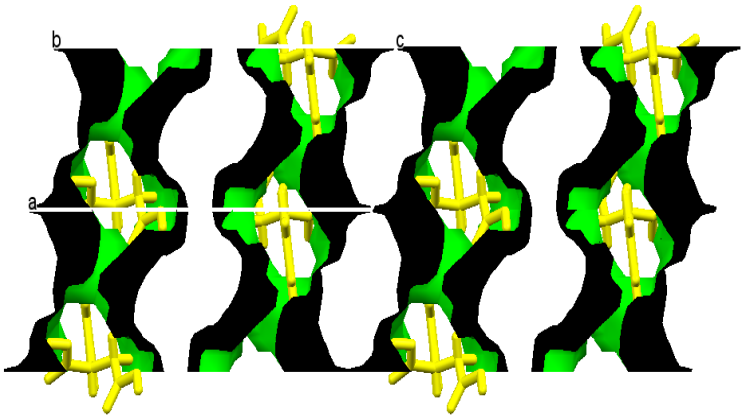
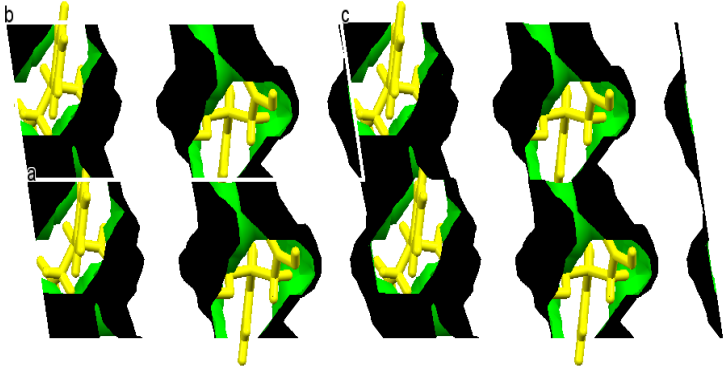
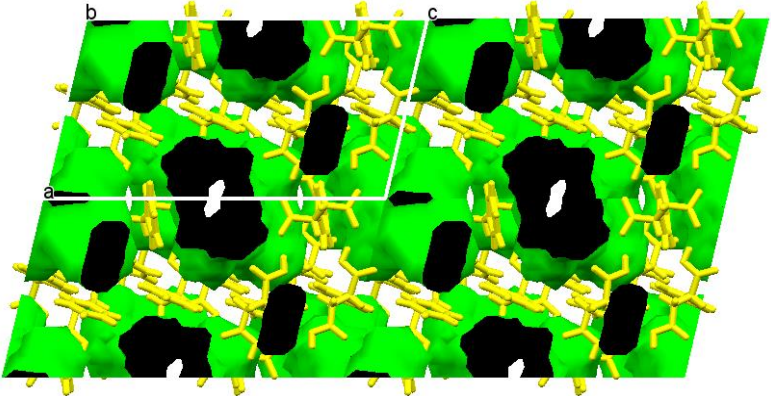
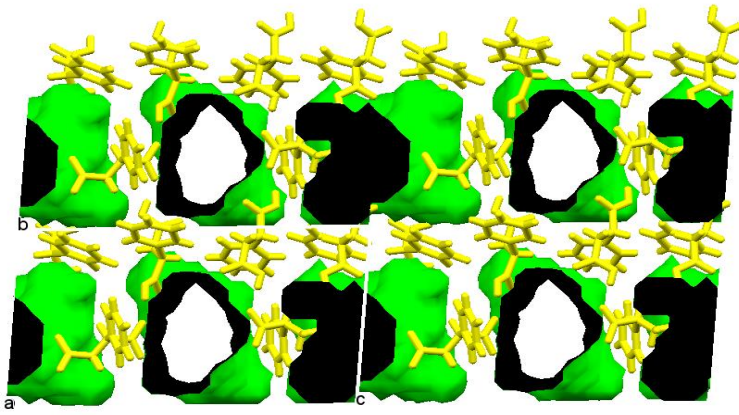
Crystal	Density	%Base	H:G ratio	Type
(R/S)-PSA·2(4PIC)	1.272 g.cm ⁻³	55.4%	1:2	Intercalate
				
(R/S)-PSA·2(2,4LUT)	1.223 g.cm ⁻³	54.6%	1:2	Intercalate
				
(R/S)-PSA·2(3,4LUT)	1.255 g.cm ⁻³	59.1%	1:2	Intercalate
				

Table S 15 Densities, voids, solvent percentages for PSA MCCs (cont.)

Crystal	Density	%Base	H:G ratio	Type
2(S)-PSA·4(3,4LUT)	1.227 g.cm ⁻³	58.1%	2:4	Intercalate
				
[(R/S)-PSA²⁺] 2[3,5LUT⁺]·2(R/S)-PSA	1.298 g.cm ⁻³	33.5%	2:3	Tubulate
				
2[(S)-PSA²⁺] 4[3,5LUT⁺]·4(S)-PSA	1.296 g.cm ⁻³	28.8%	4:6	Tubulate
				

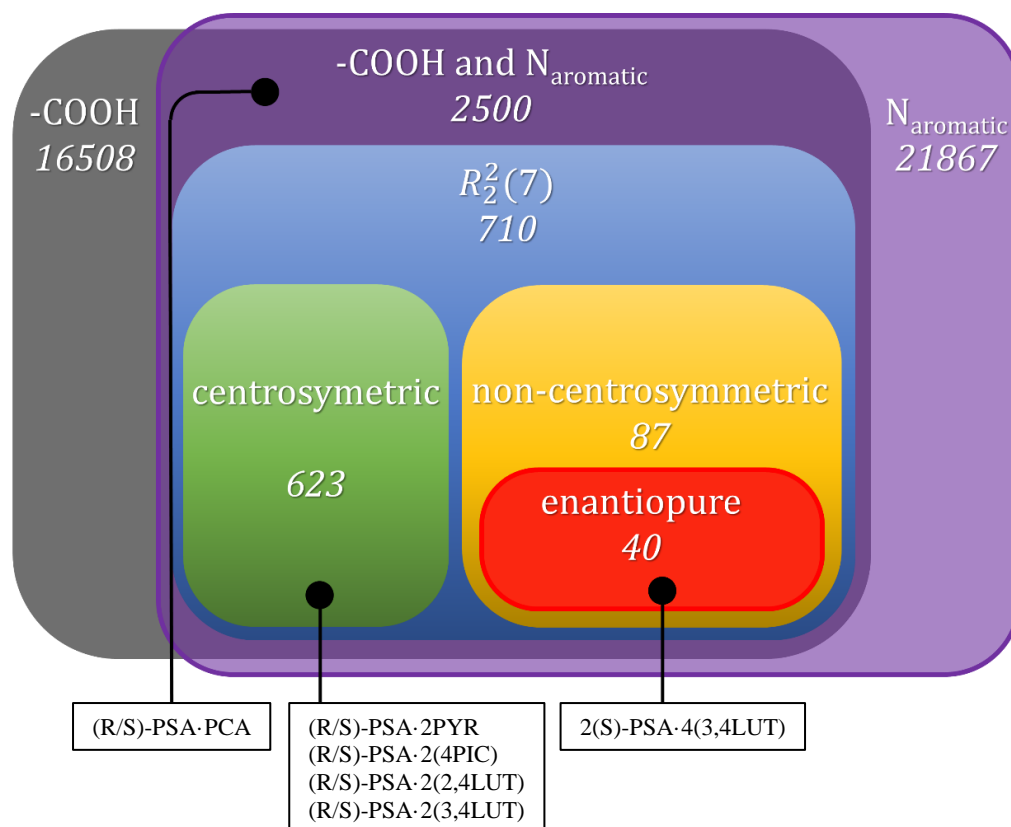


Figure S 3 Occurrence of carboxylic acid and pyridine moieties, and their combination in the CSD

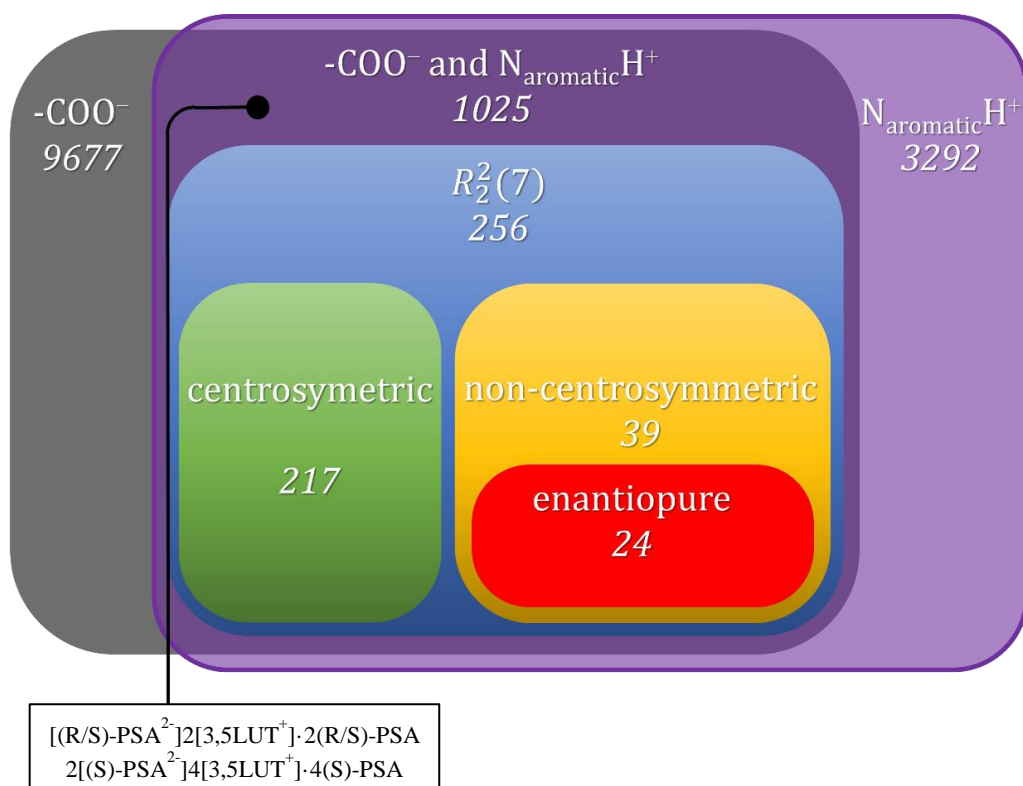


Figure S 4 Occurrence of carboxylate and pyridinium moieties, and their combination in the CSD

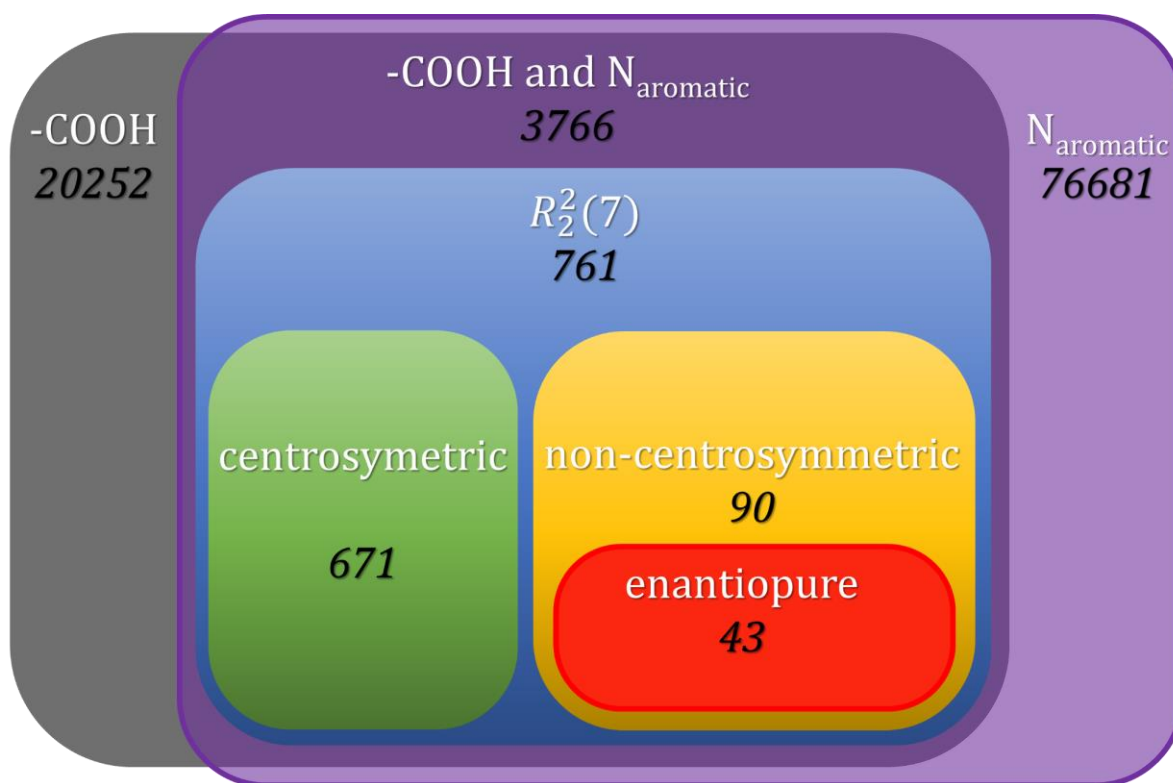


Figure S 5 Occurrence of carboxylic acid and pyridine moieties, and their combination in the CSD (Organic & Inorganic)

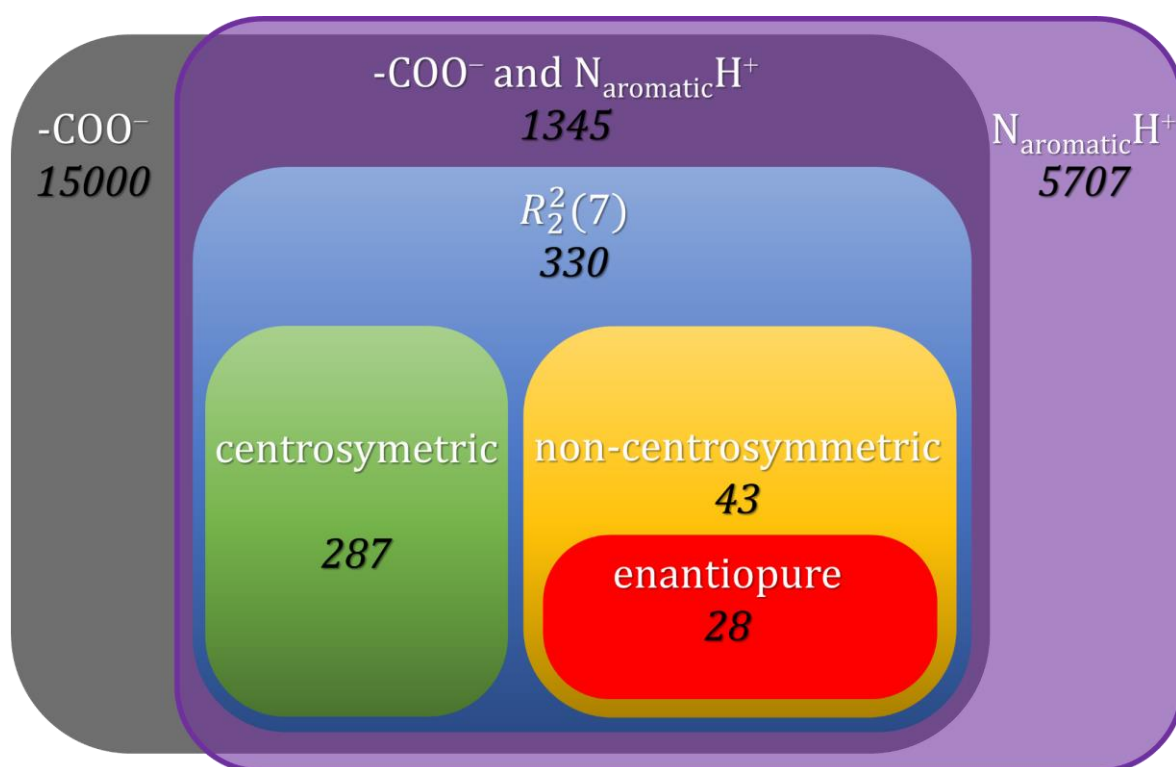


Figure S 6 Occurrence of carboxylate and pyridinium moieties, and their combination in the CSD (Organic & Inorganic)

Results of bulk property analysis (DSC, TGA, PXRD and FTIR) for all MCCs of PSA

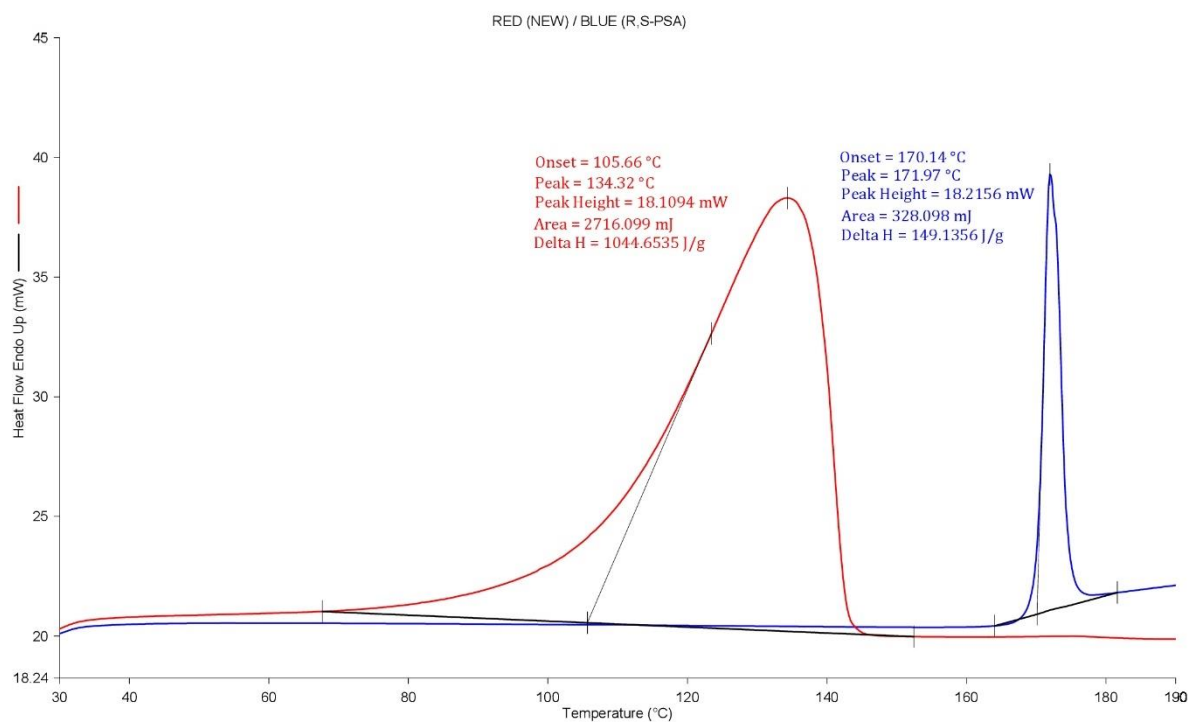


Figure S7 DSC curve of $[2\text{tBa}^+][\text{COO}^{2-}]$ and the starting material

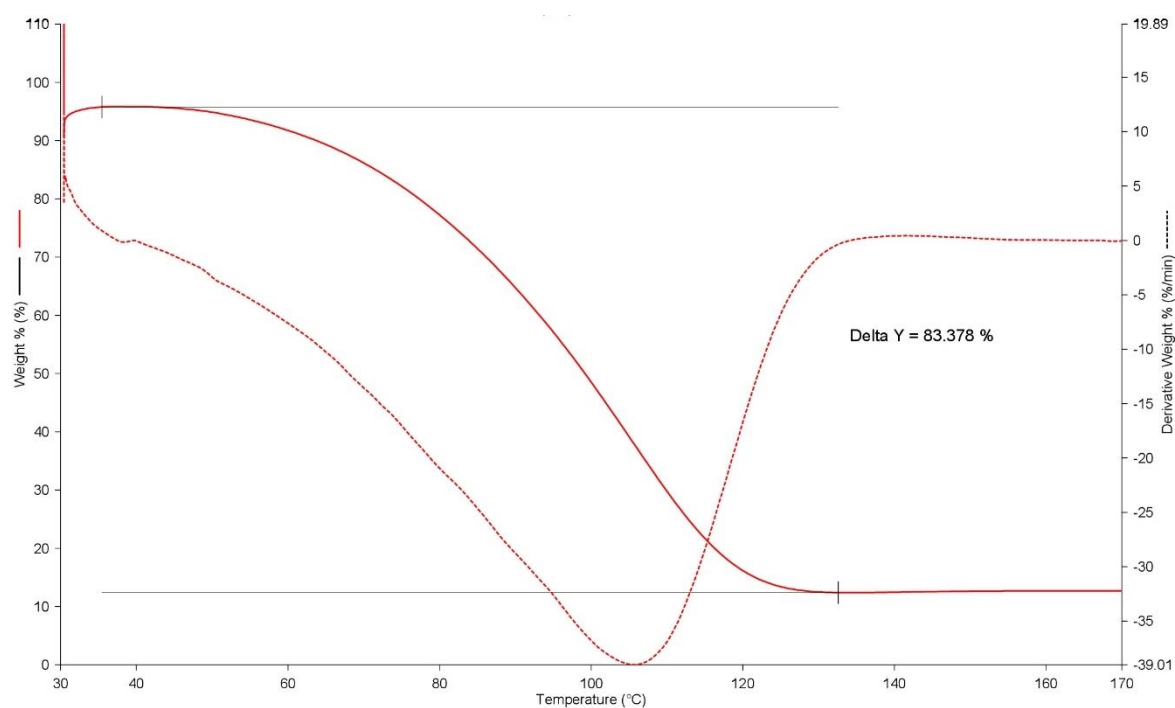


Figure S8 TG curve of $[2\text{tBa}^+][\text{COO}^{2-}]$

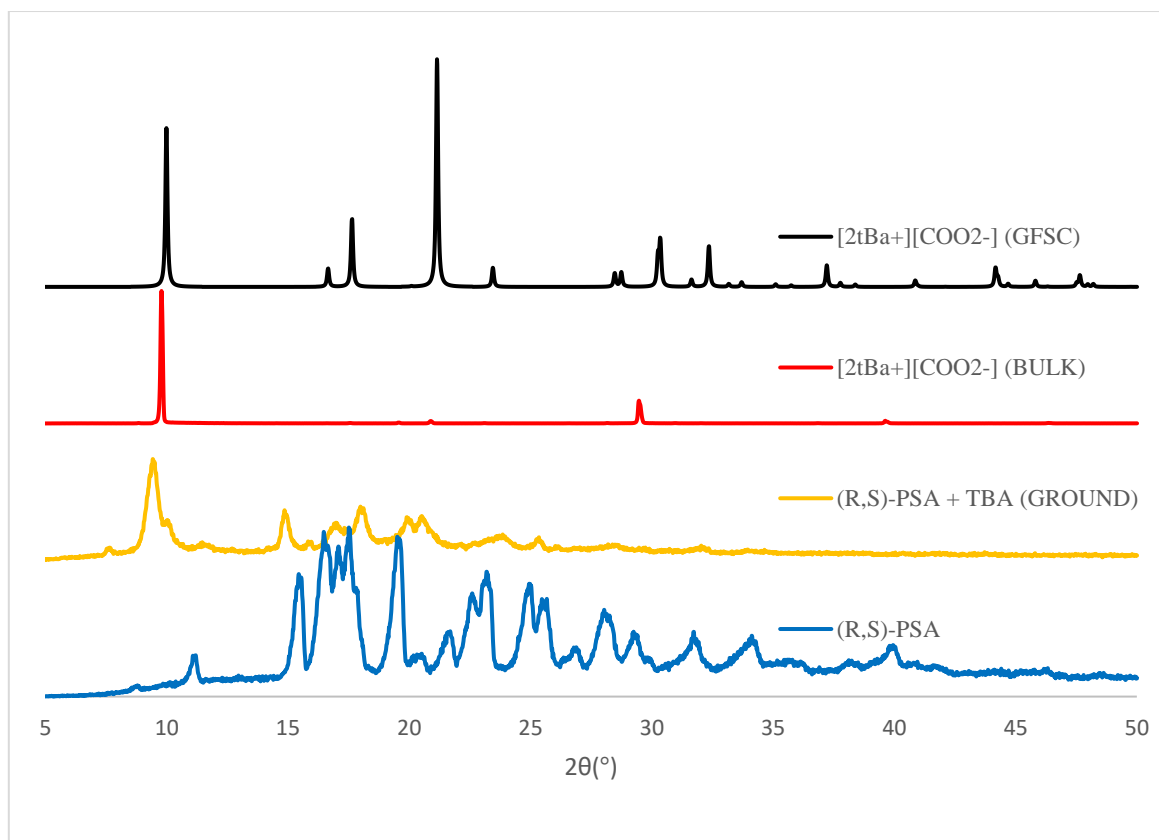


Figure S9 PXRD curve of [2tBa⁺][COO²⁻] and the starting material

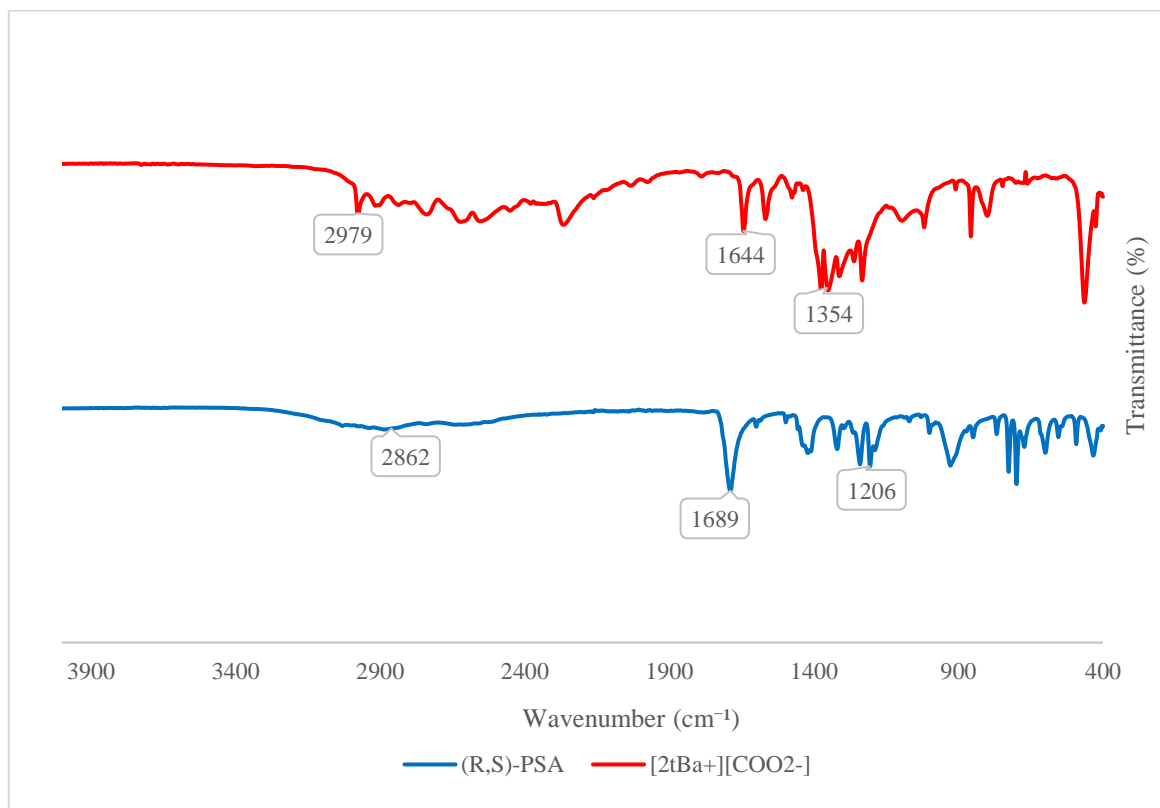


Figure S10 IR curve of [2tBa⁺][COO²⁻] and the starting material

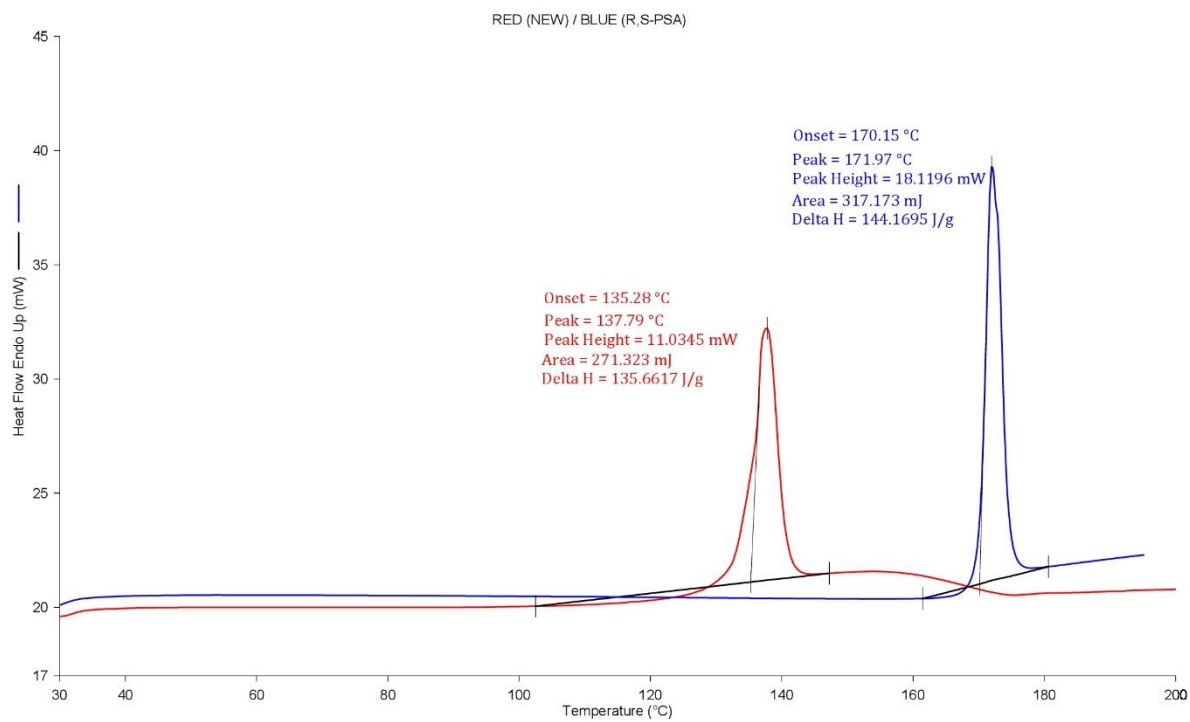


Figure S11 DSC curve of [(R/S)-PSA⁻][ANI⁺] and the starting material

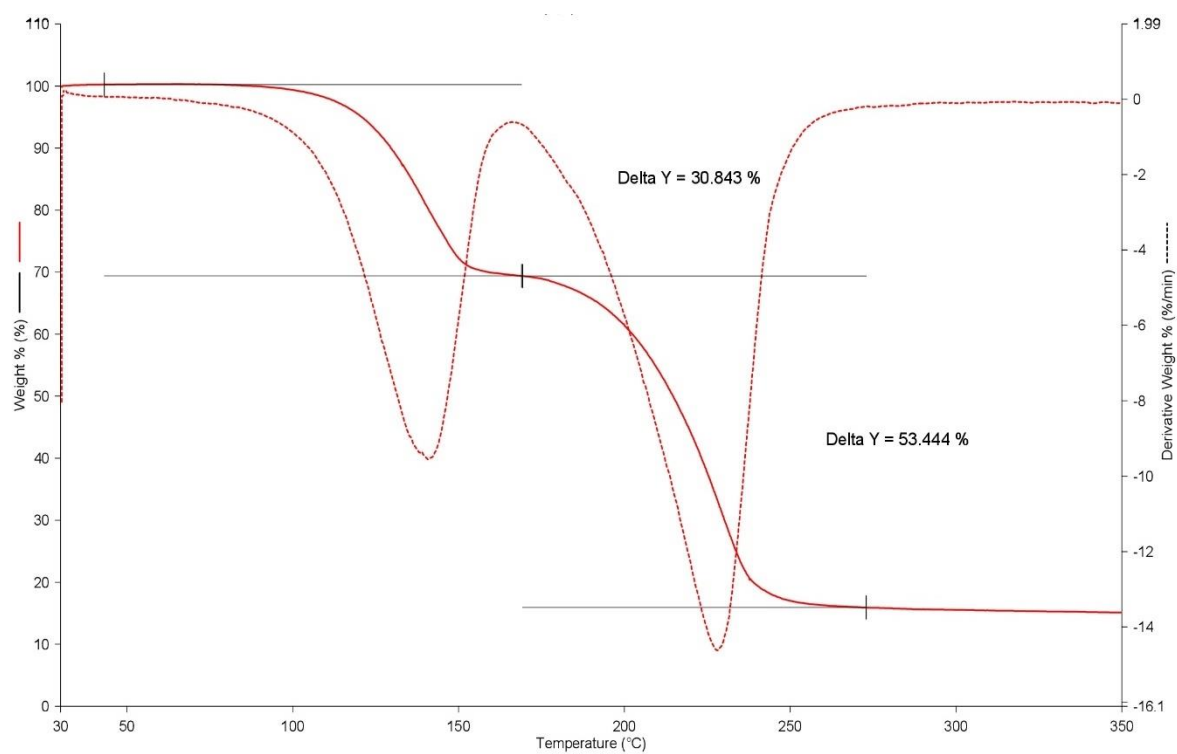


Figure S12 TG curve of [(R/S)-PSA⁻][ANI⁺]

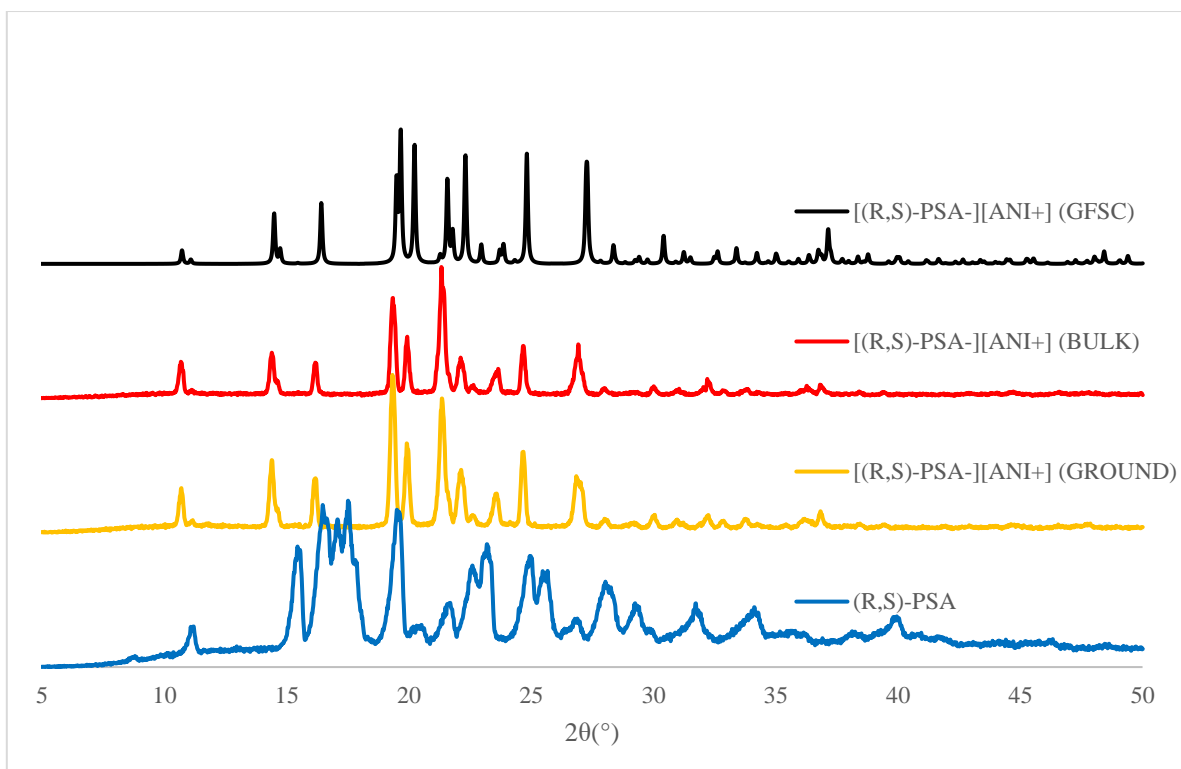


Figure S13 PXRD curve of $[(R,S)\text{-PSA}^-][\text{ANI}^+]$ and the starting material

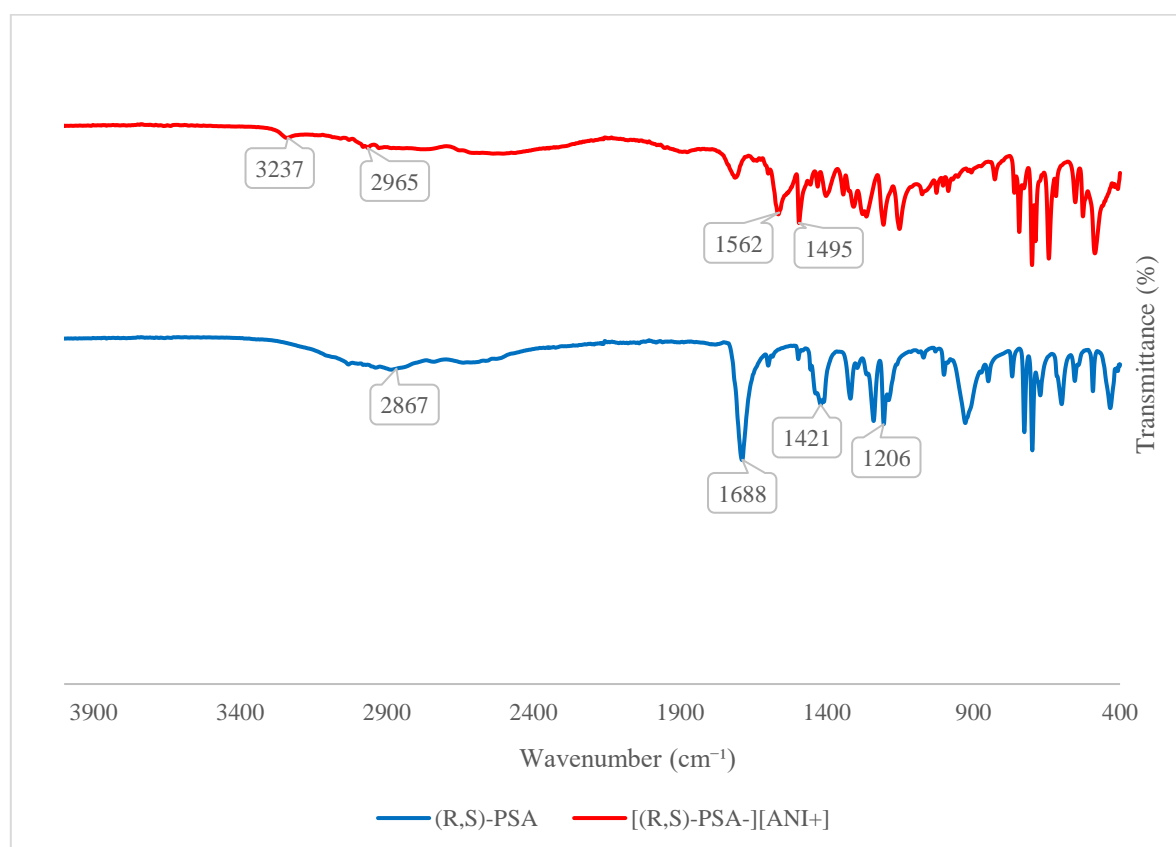


Figure S14 IR curve of $[(R,S)\text{-PSA}^-][\text{ANI}^+]$ and the starting material

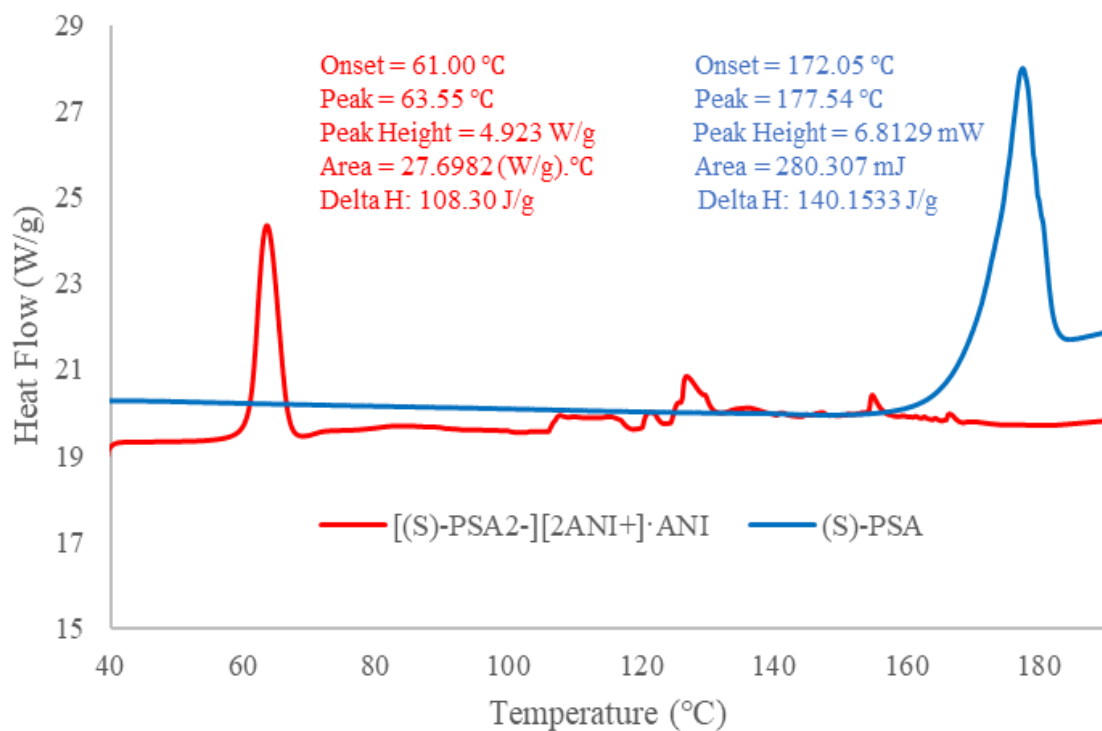


Figure S15 DSC curve of [(S)-PSA²⁻][2ANI⁺]·ANI and the starting material

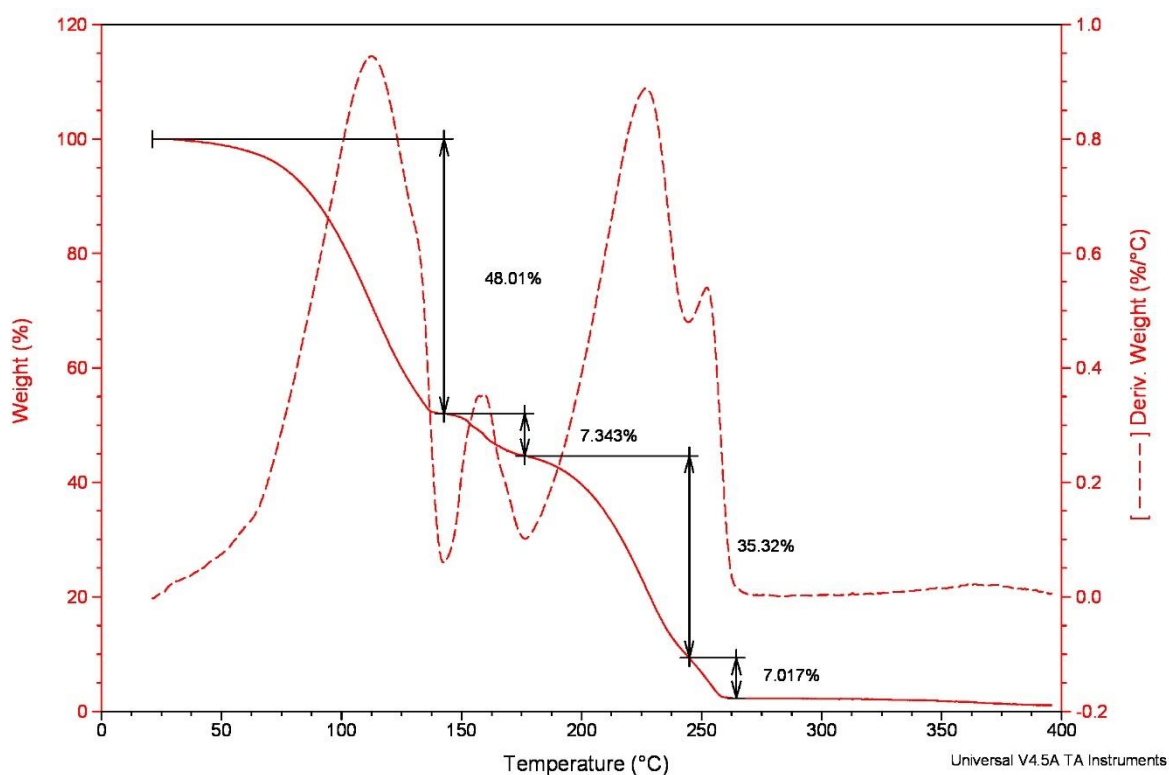


Figure S16 TG curve of [(S)-PSA²⁻][2ANI⁺]·ANI

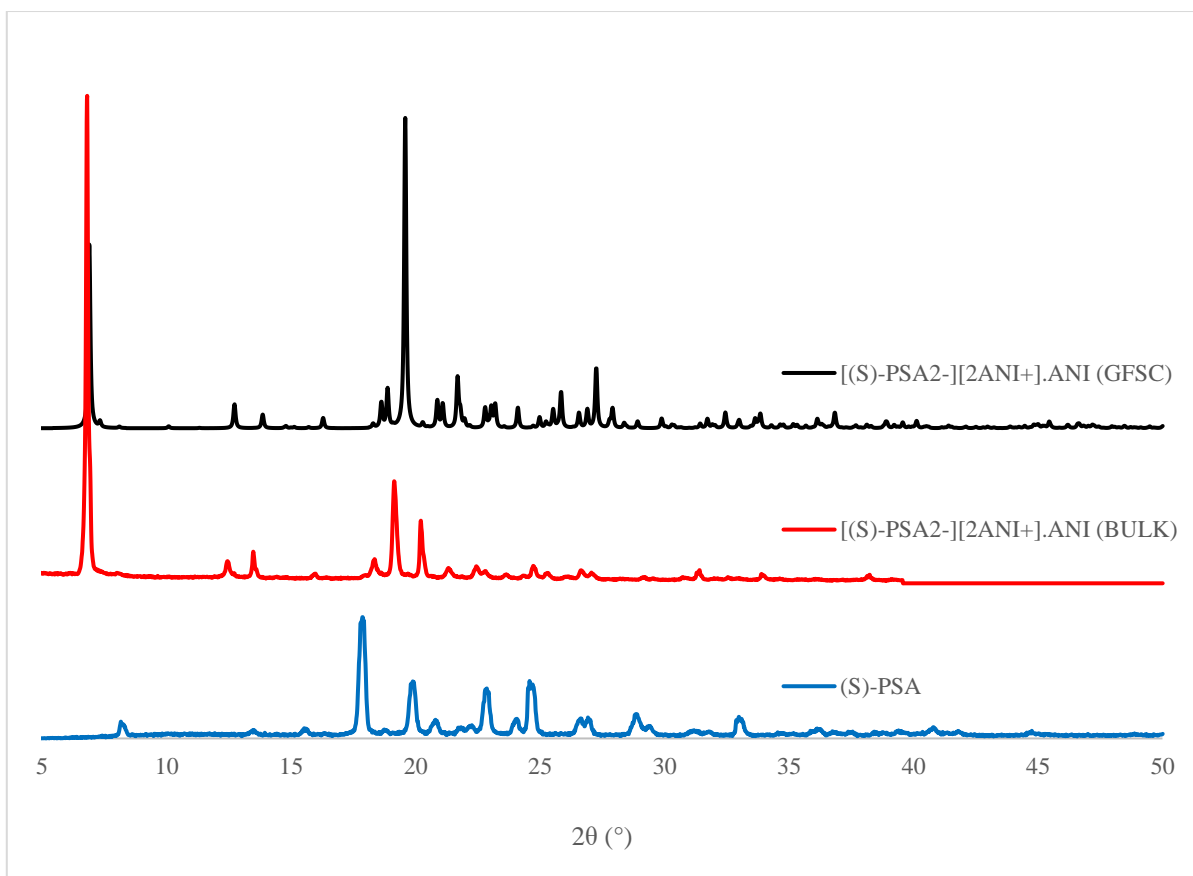


Figure S17 PXRD curve of $[(S)\text{-PSA}^{2-}][2\text{ANI}^+]\cdot\text{ANI}$ and the starting material

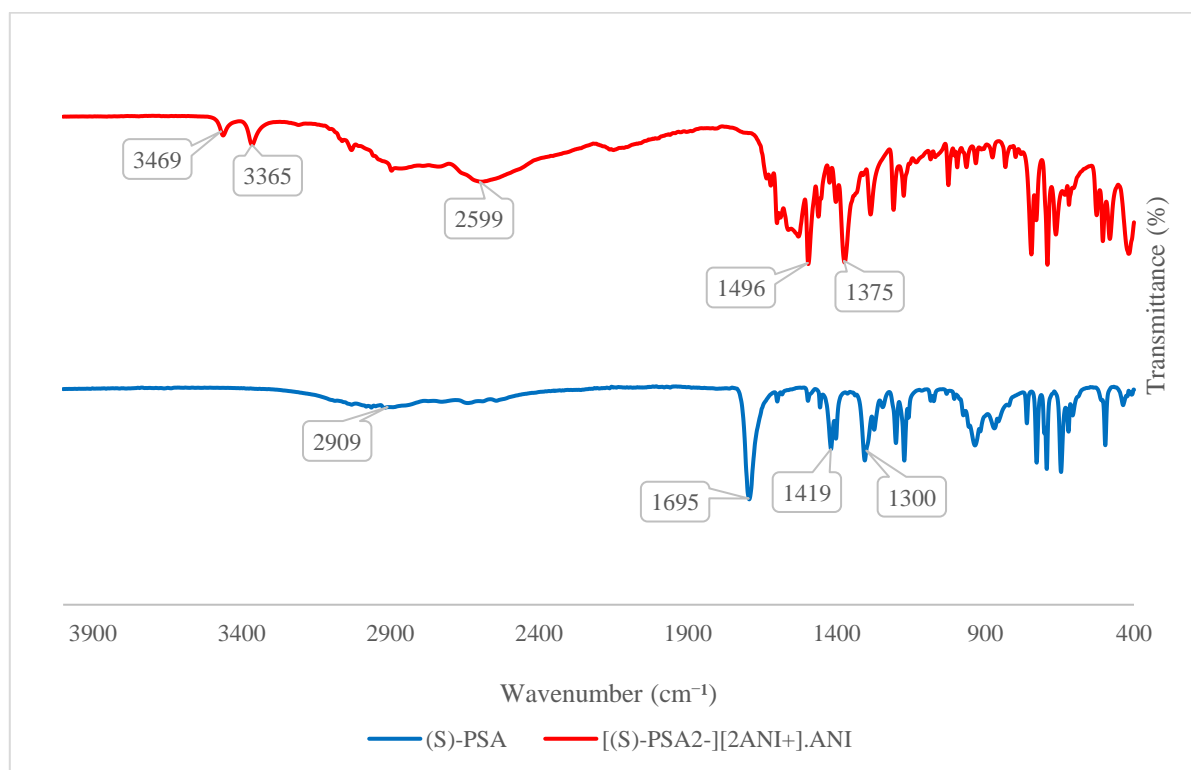


Figure S18 IR curve of $[(S)\text{-PSA}^{2-}][2\text{ANI}^+]\cdot\text{ANI}$ and the starting material

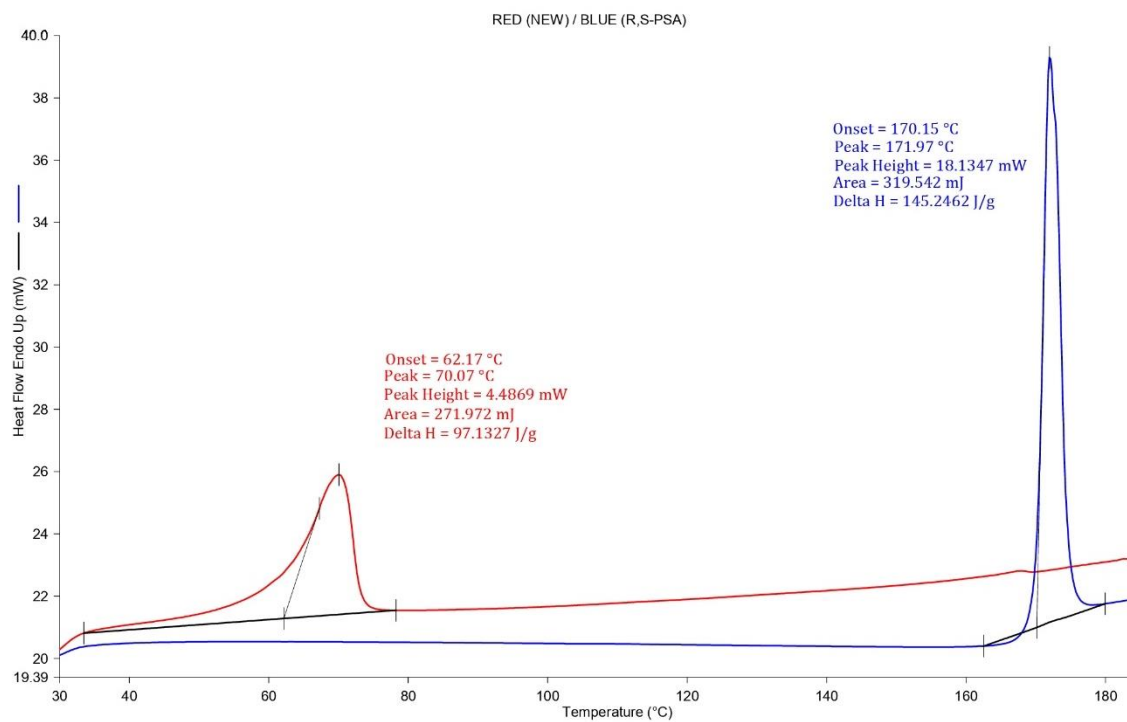


Figure S19 DSC curve of (R/S)-PSA·2PYR and the starting material

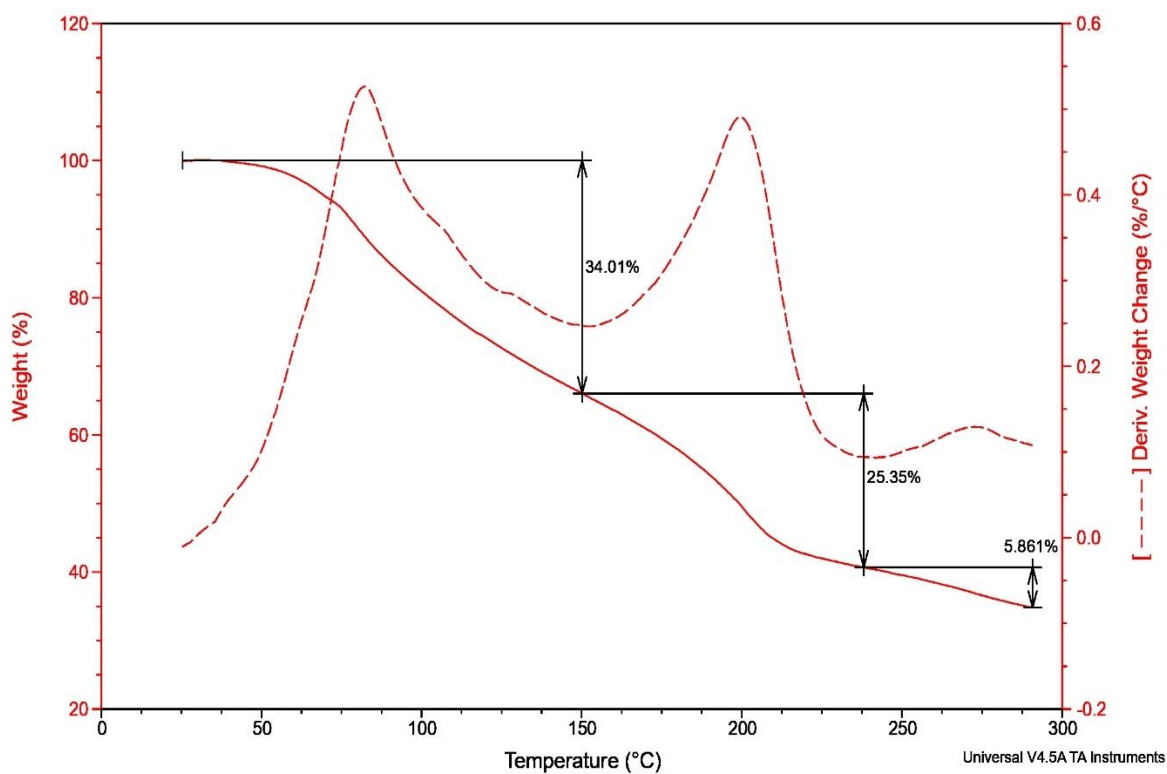


Figure S20 TG curve of (R/S)-PSA·2PYR

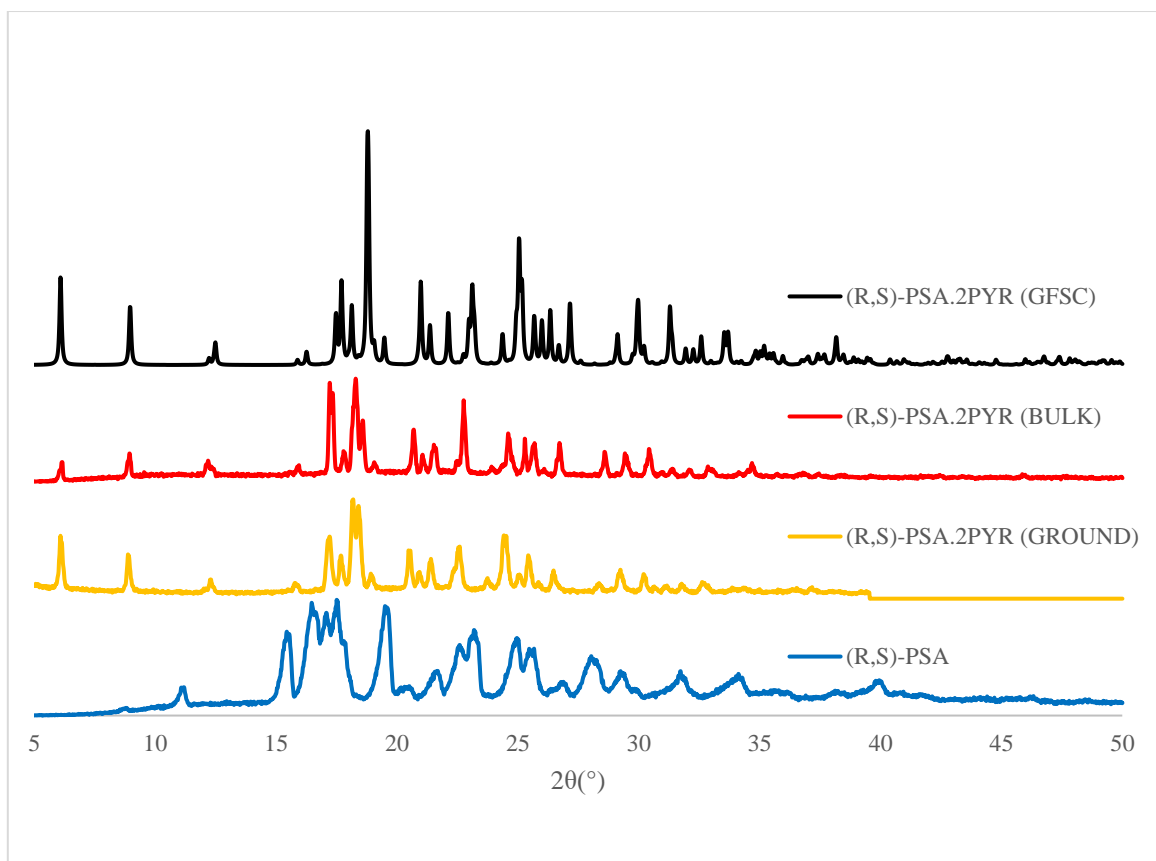


Figure S21 PXRD curve of (R/S)-PSA·2PYR and the starting material

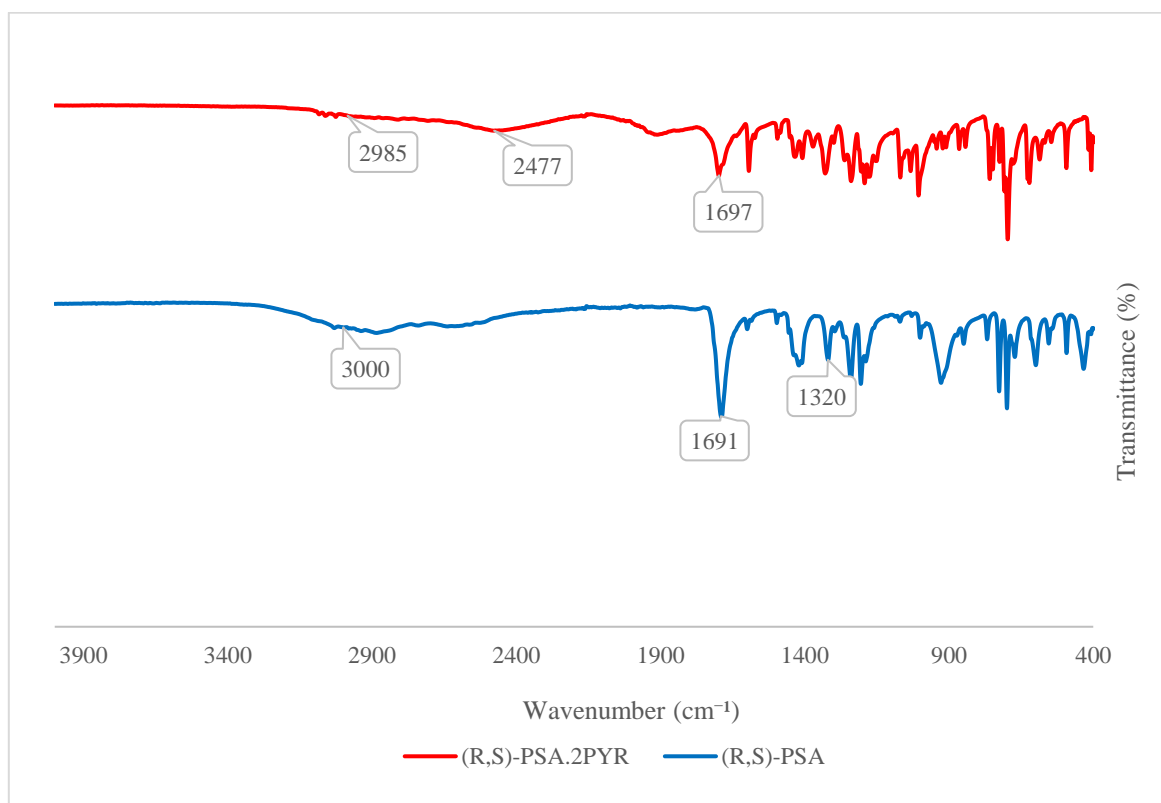


Figure S22 IR curve of (R/S)-PSA·2PYR and the starting material

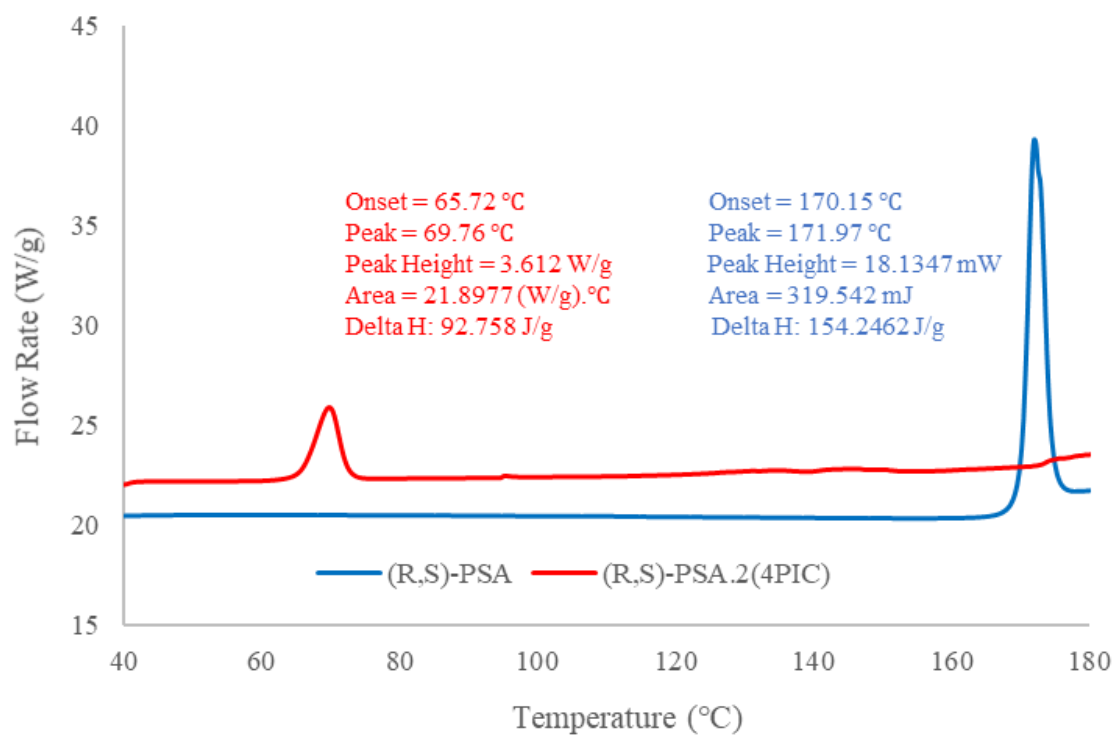


Figure S23 DSC curve of (R/S)-PSA·2(4PIC) and the starting material

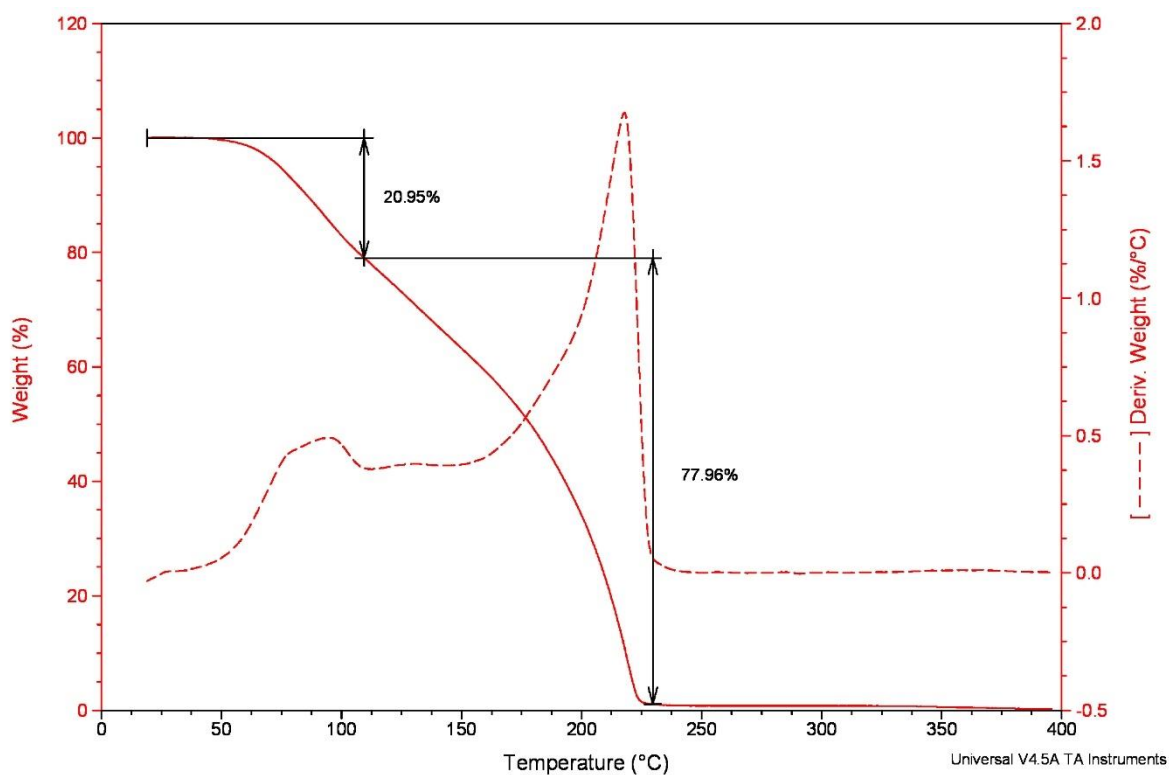


Figure S24 TG curve of (R/S)-PSA·2(4PIC)

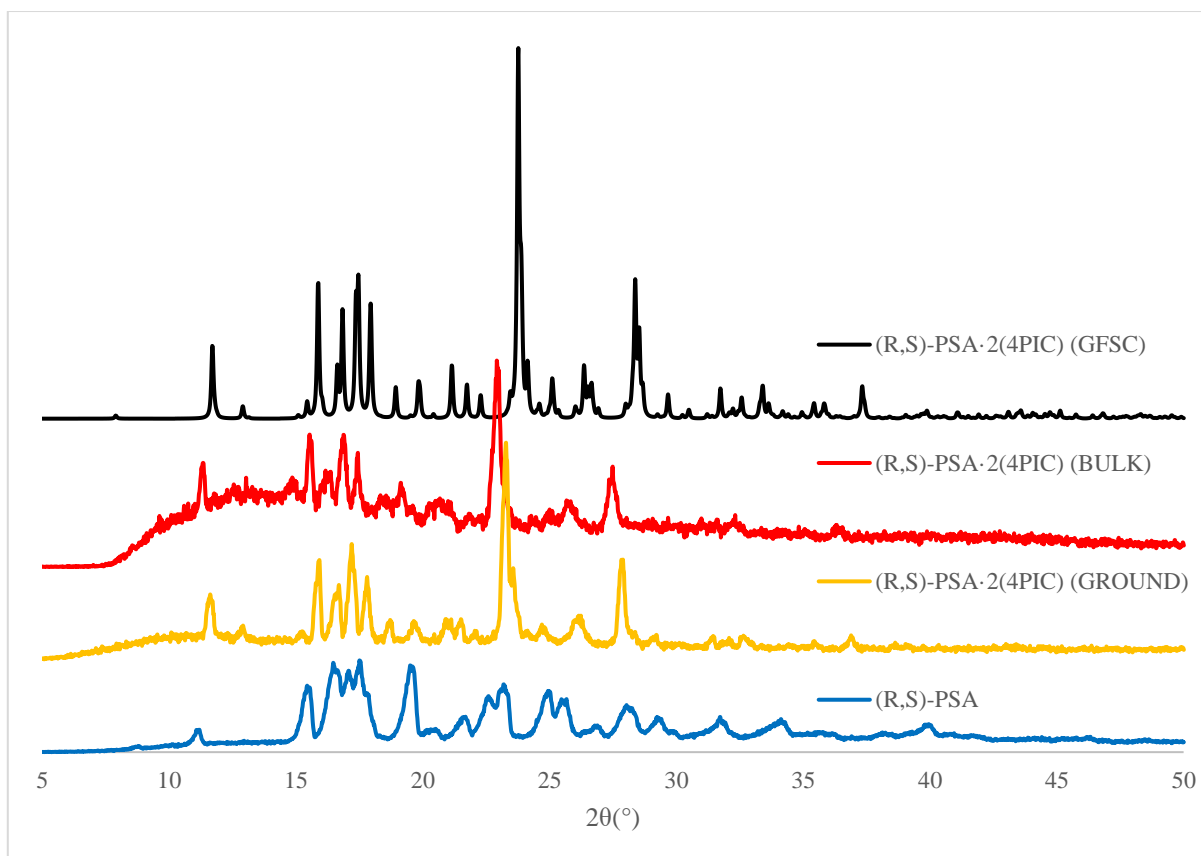


Figure S25 PXRD curve of (R/S)-PSA·2(4PIC) and the starting material

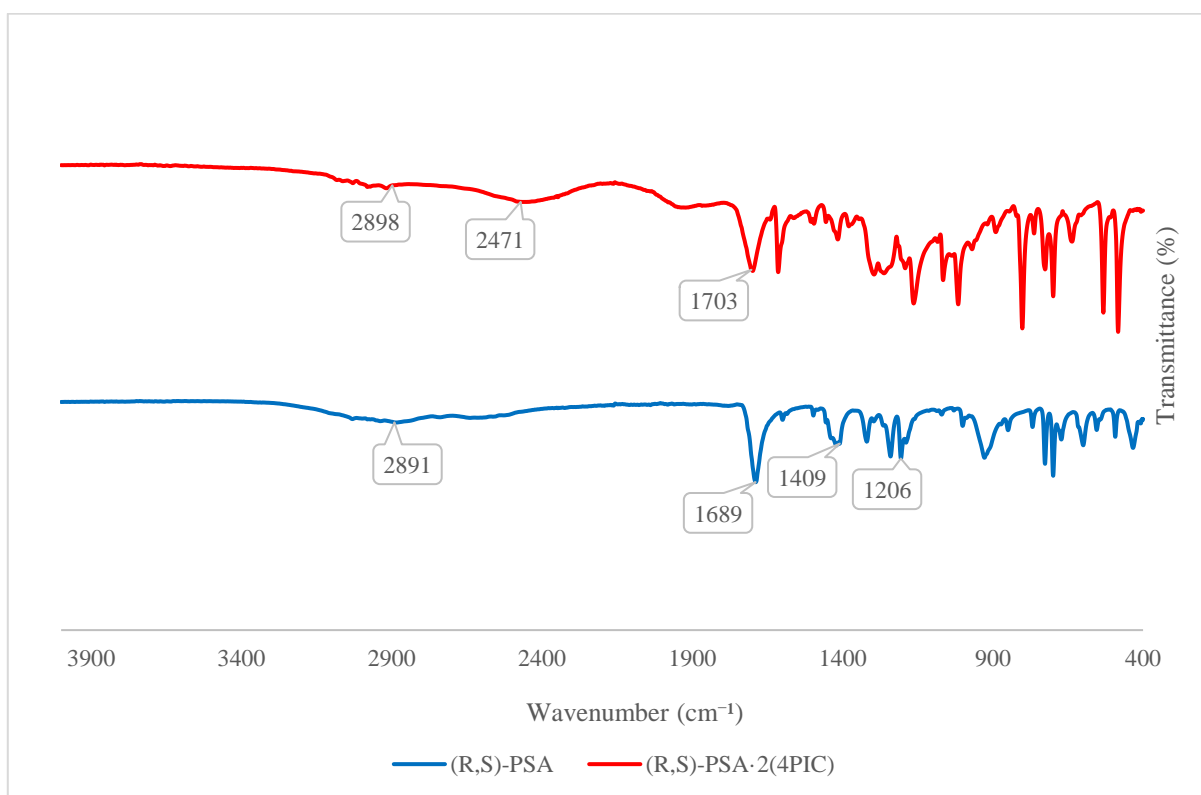


Figure S26 IR curve of (R/S)-PSA·2(4PIC) and the starting material

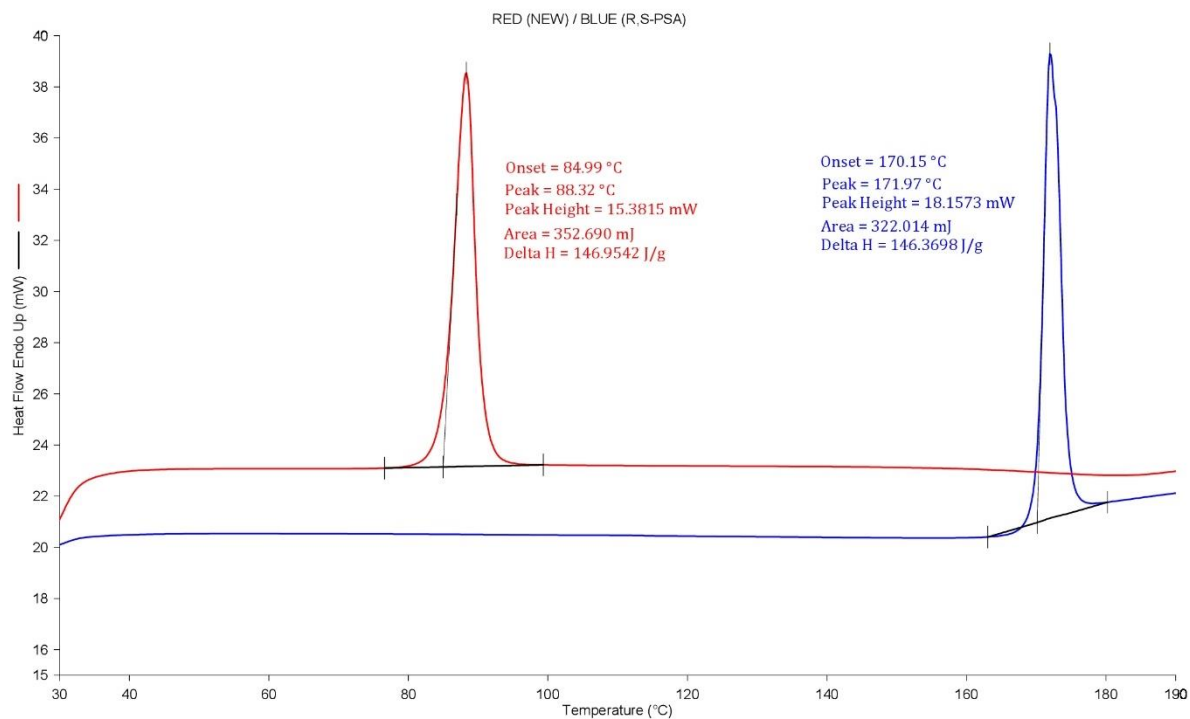


Figure S27 DSC curve of (R/S)-PSA·2(3,4LUT) and the starting material

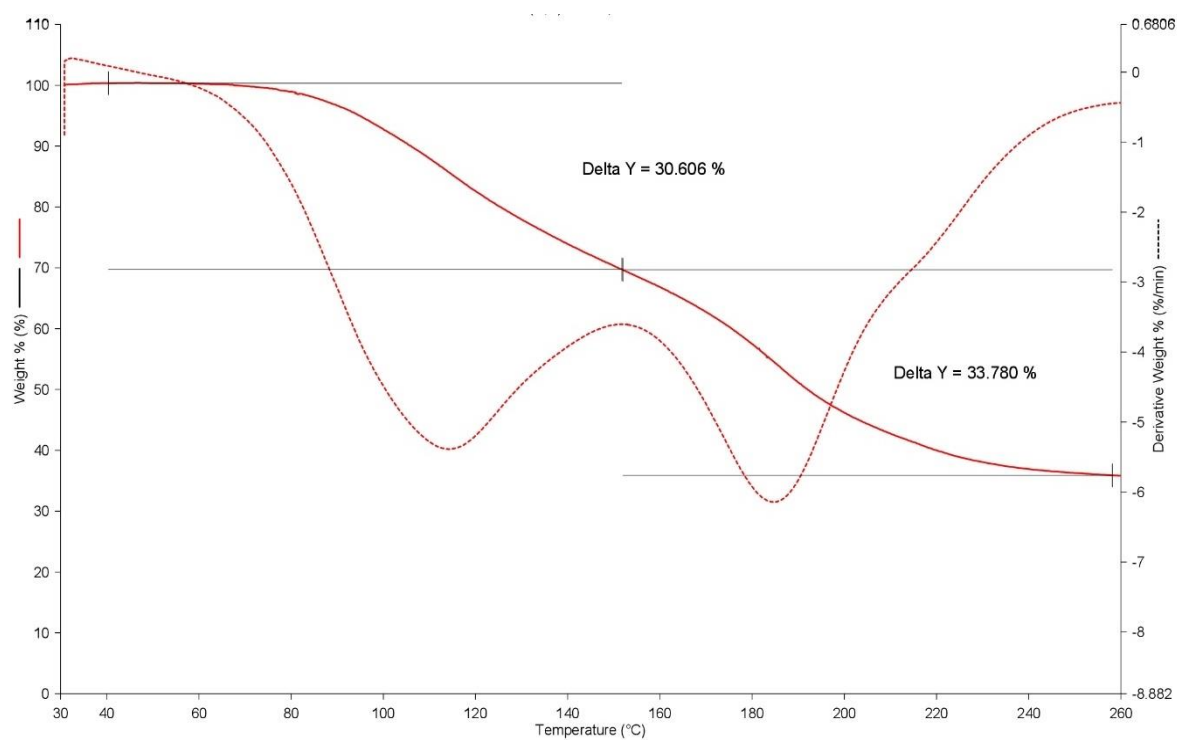


Figure S28 TG curve of (R/S)-PSA·2(3,4LUT)

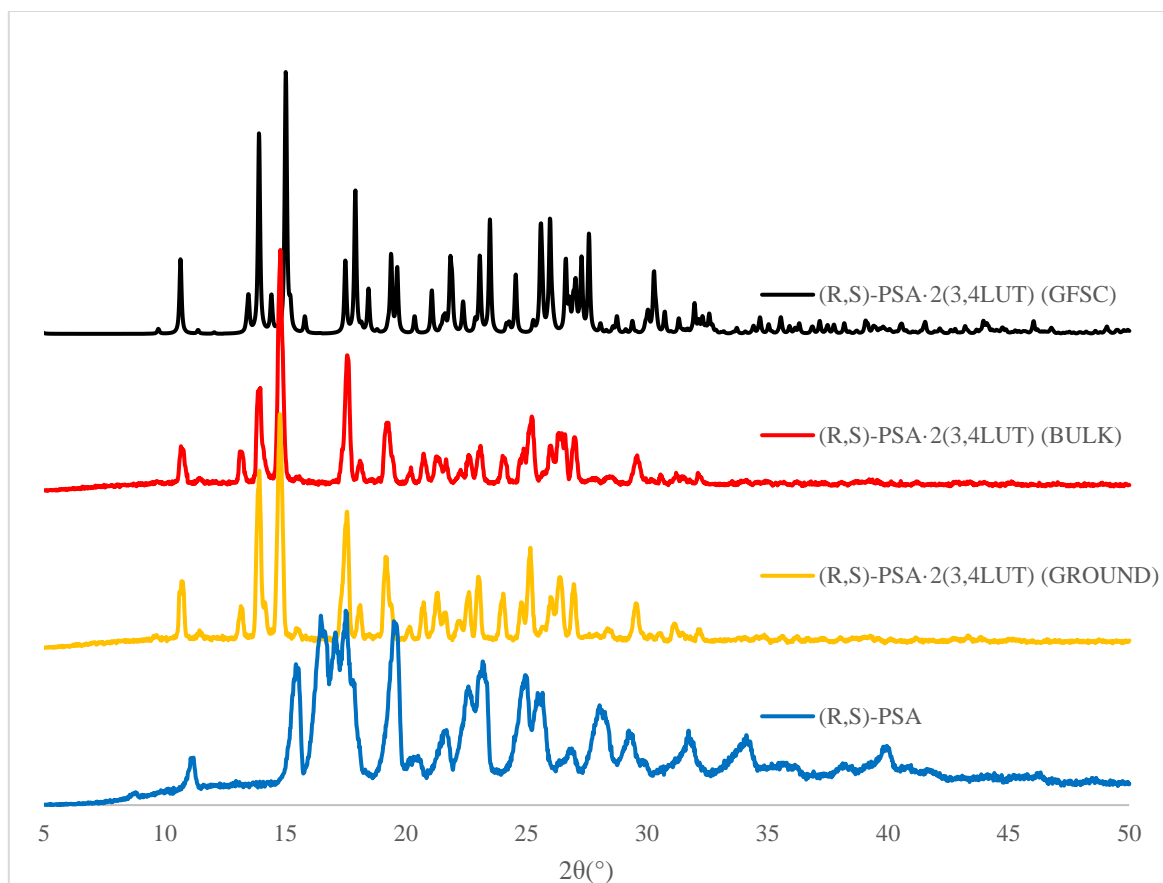


Figure S29 PXRD curve of (R/S)-PSA·2(3,4LUT) and the starting material

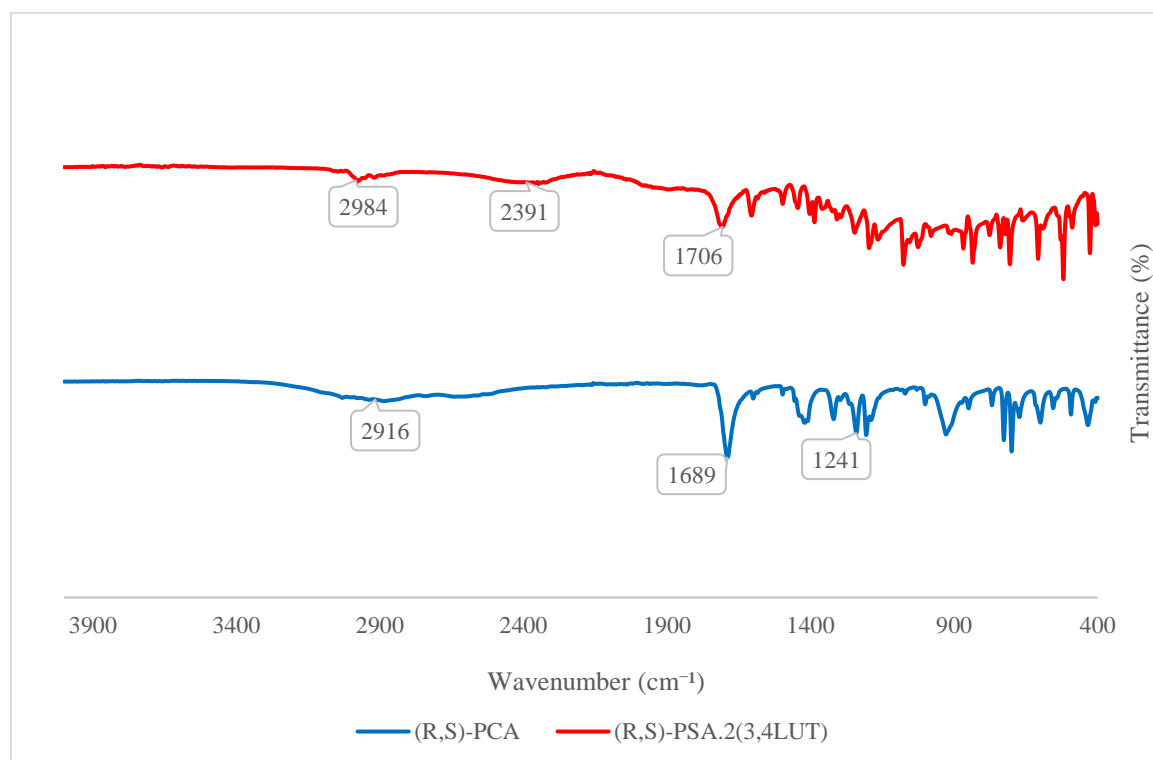


Figure S30 IR curve of (R/S)-PSA·2(3,4LUT) and the starting material

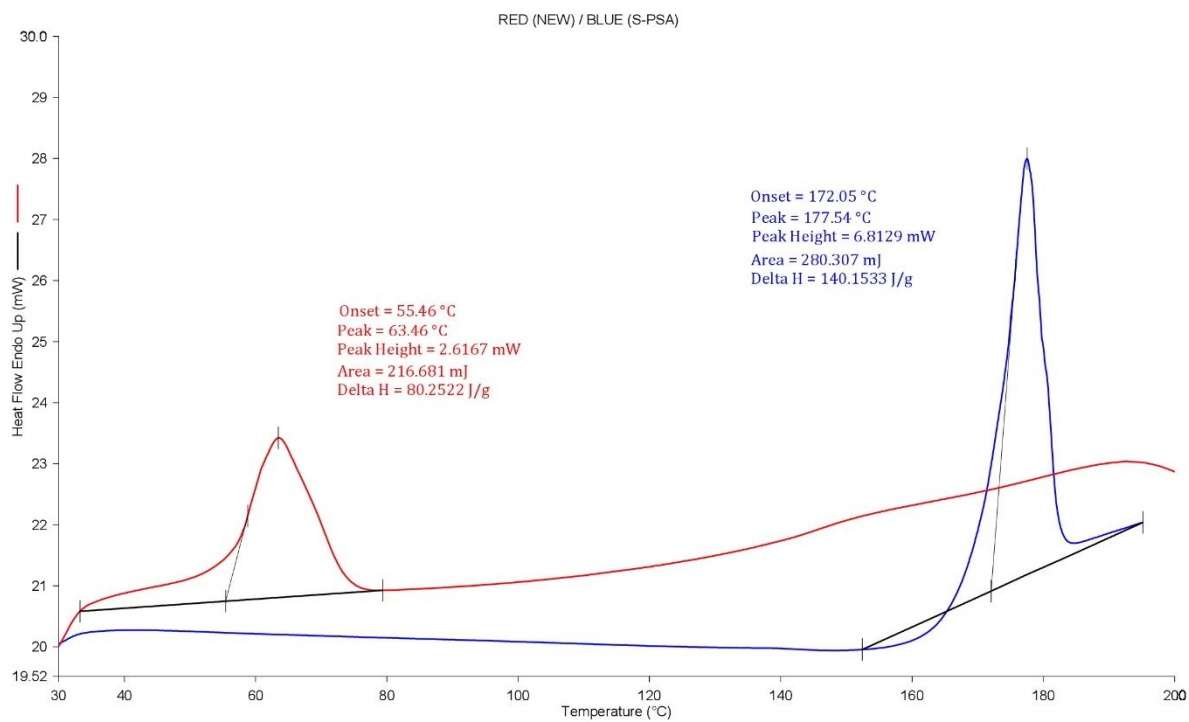


Figure S31 DSC curve of 2(S)-PSA·4(3,4LUT) and the starting material

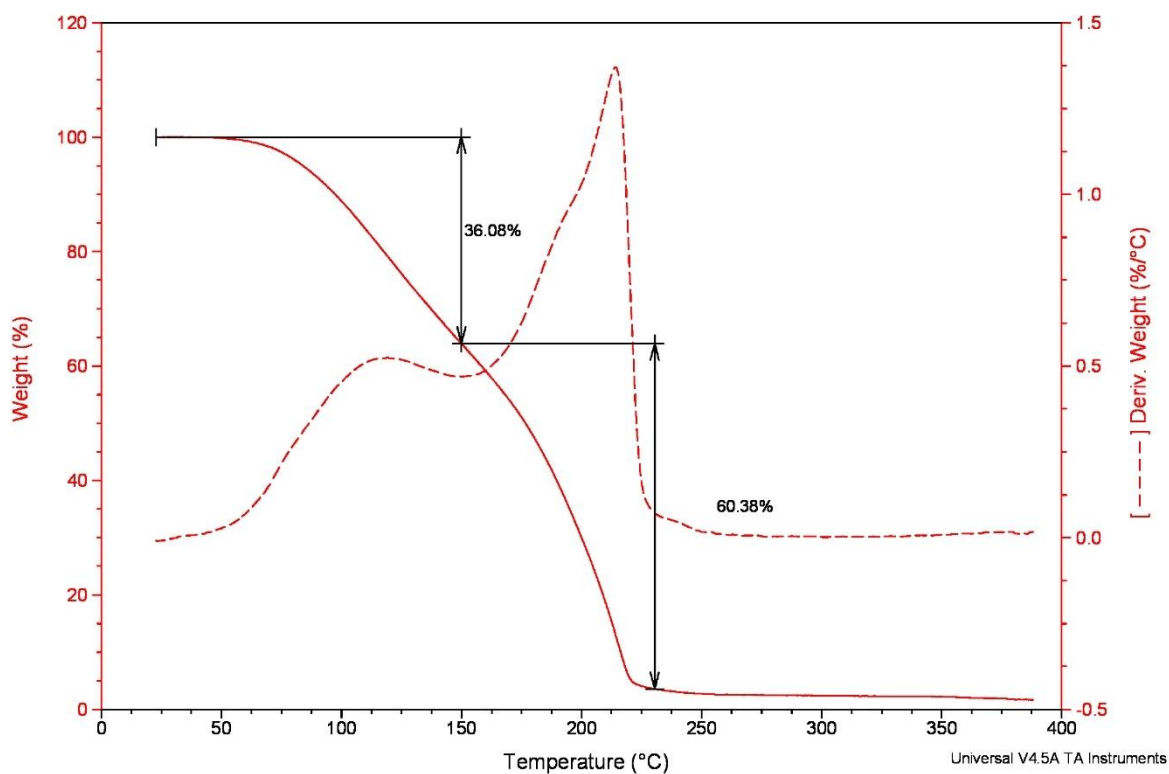


Figure S32 TG curve of 2(S)-PSA·4(3,4LUT)

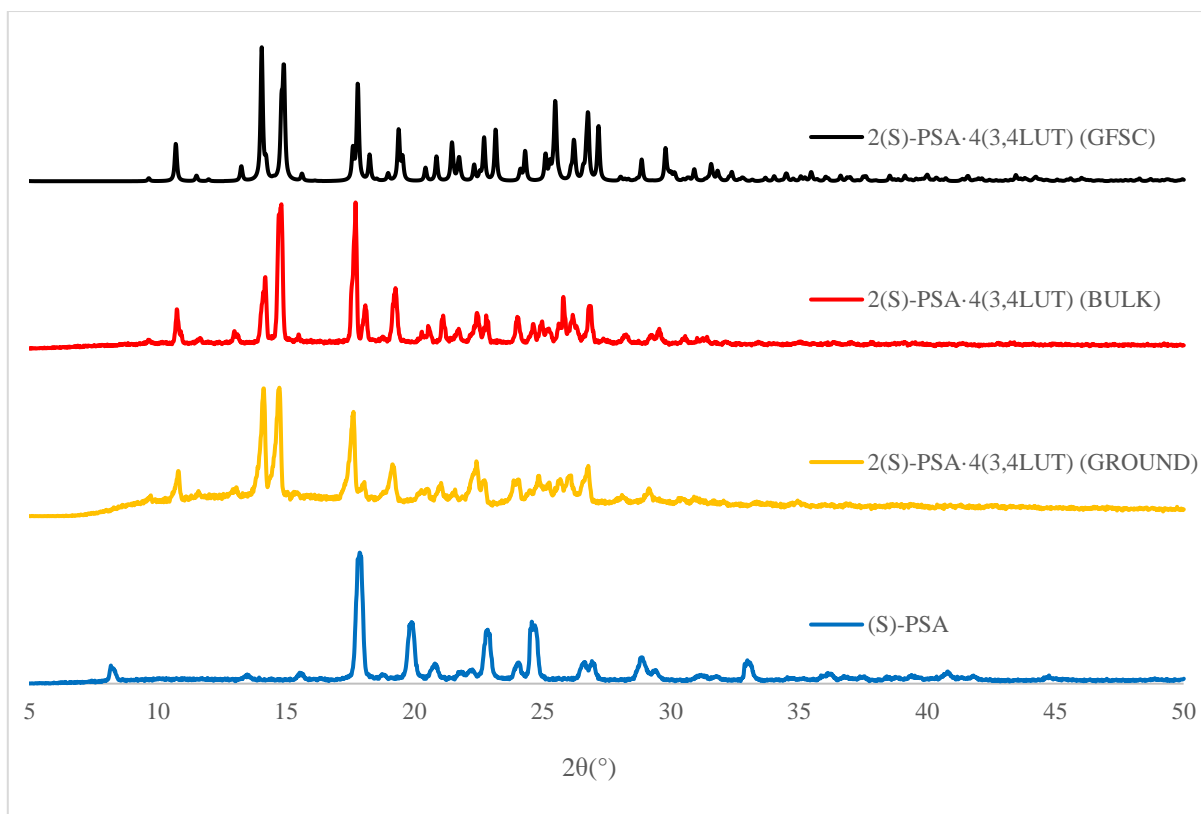


Figure S33 PXRD curve of 2(S)-PSA·4(3,4LUT) and the starting material

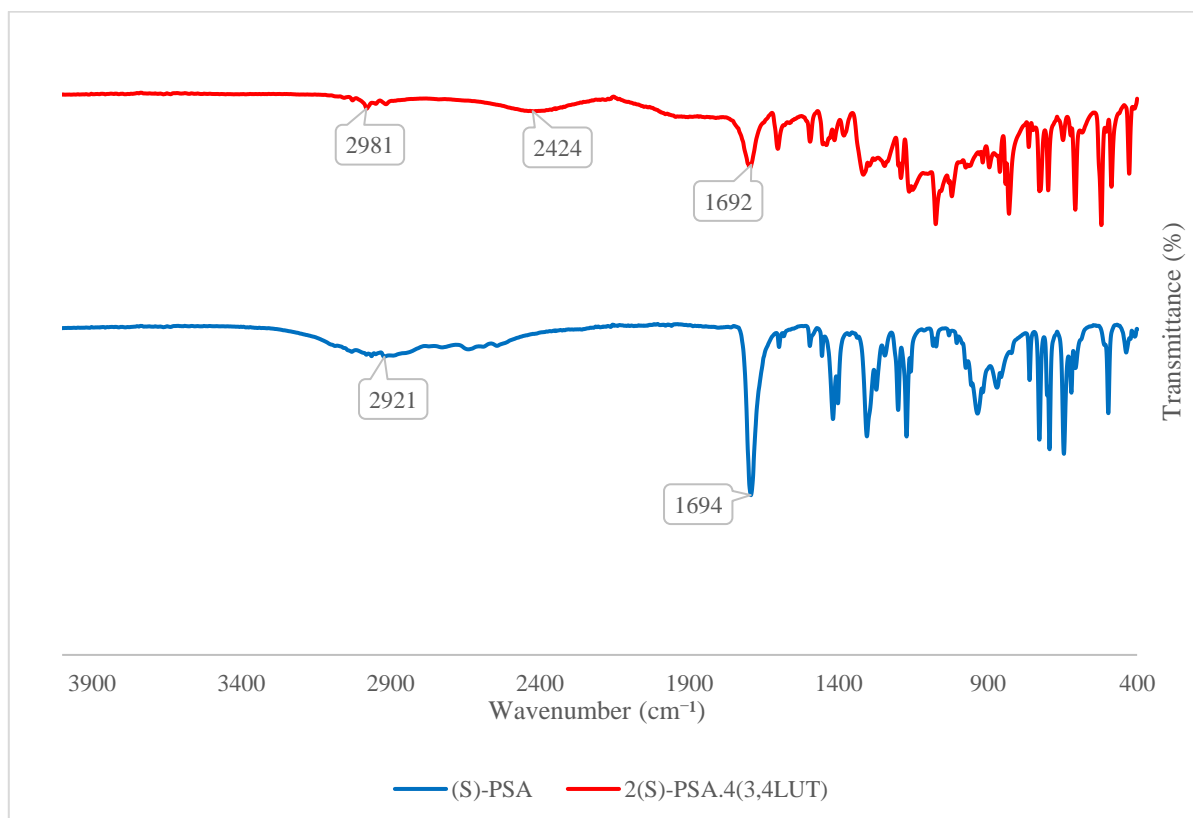


Figure S34 IR curve of 2(S)-PSA·4(3,4LUT) and the starting material

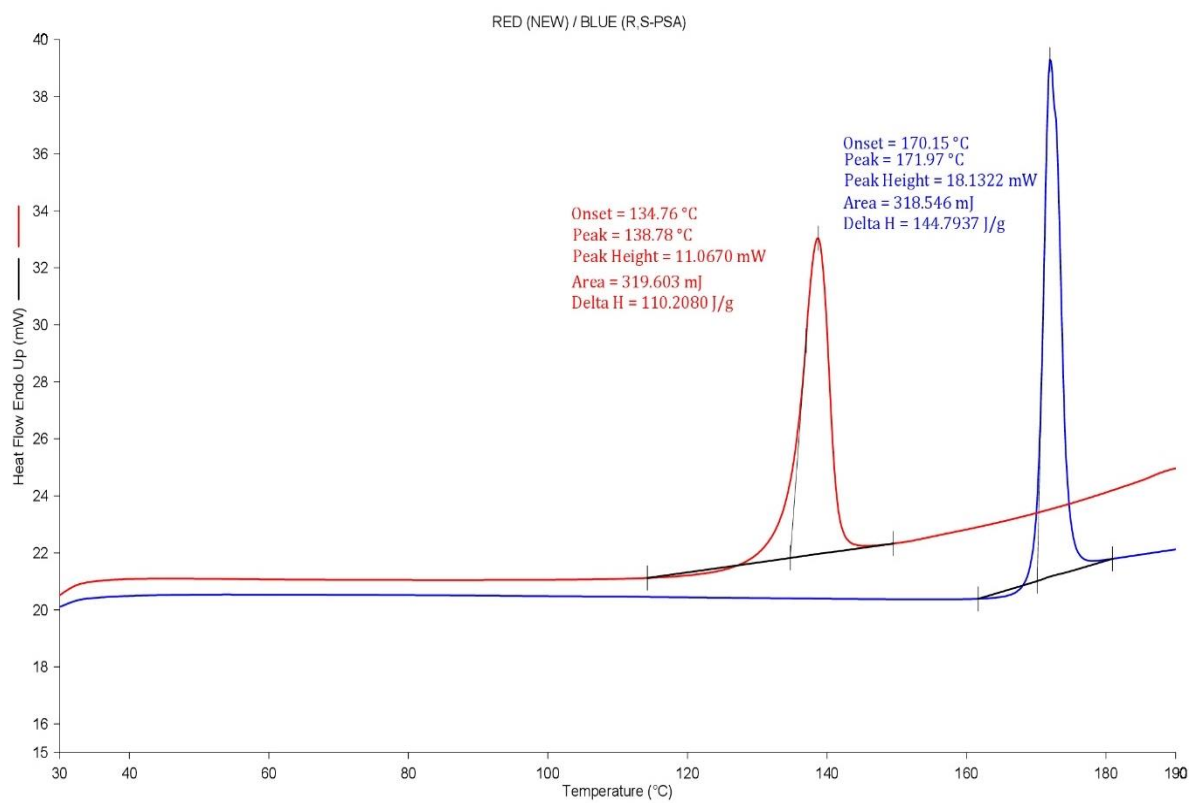


Figure S35 DSC curve of $[(R/S)\text{-PSA}^{2-}] \cdot 2[3,5\text{LUT}^+] \cdot 2(R/S)\text{-PSA}$ and the starting material

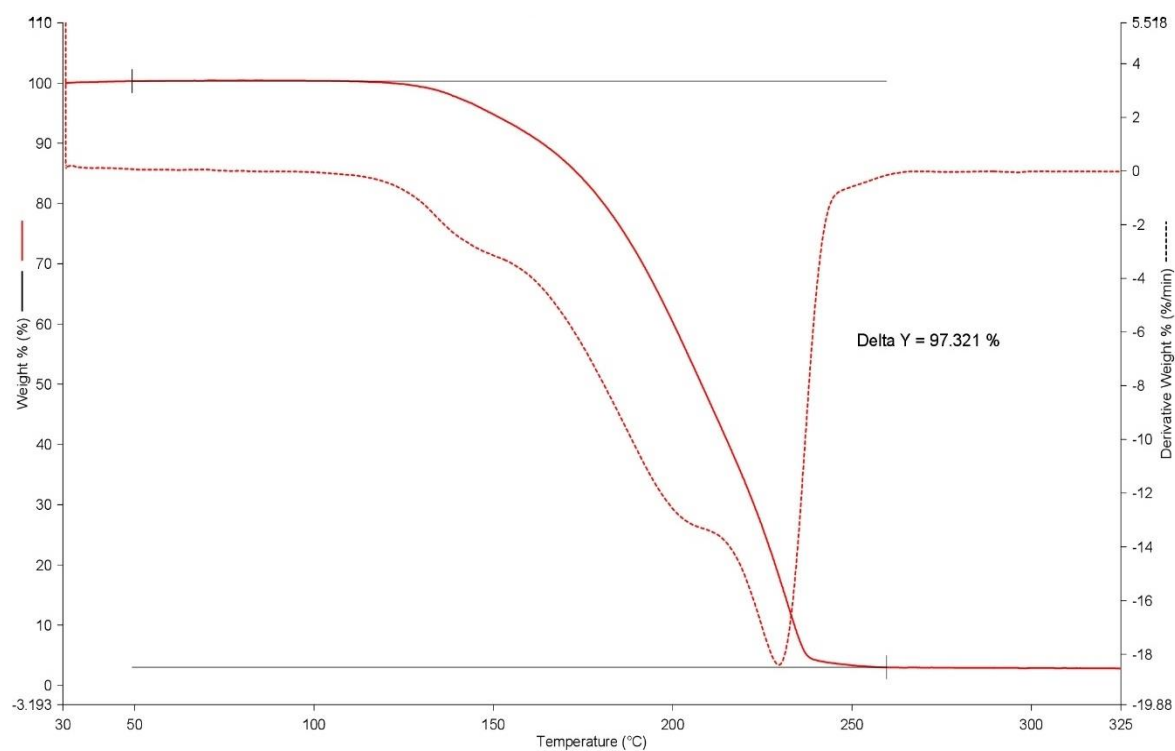


Figure S36 TG curve of $[(R/S)\text{-PSA}^{2-}] \cdot 2[3,5\text{LUT}^+] \cdot 2(R/S)\text{-PSA}$

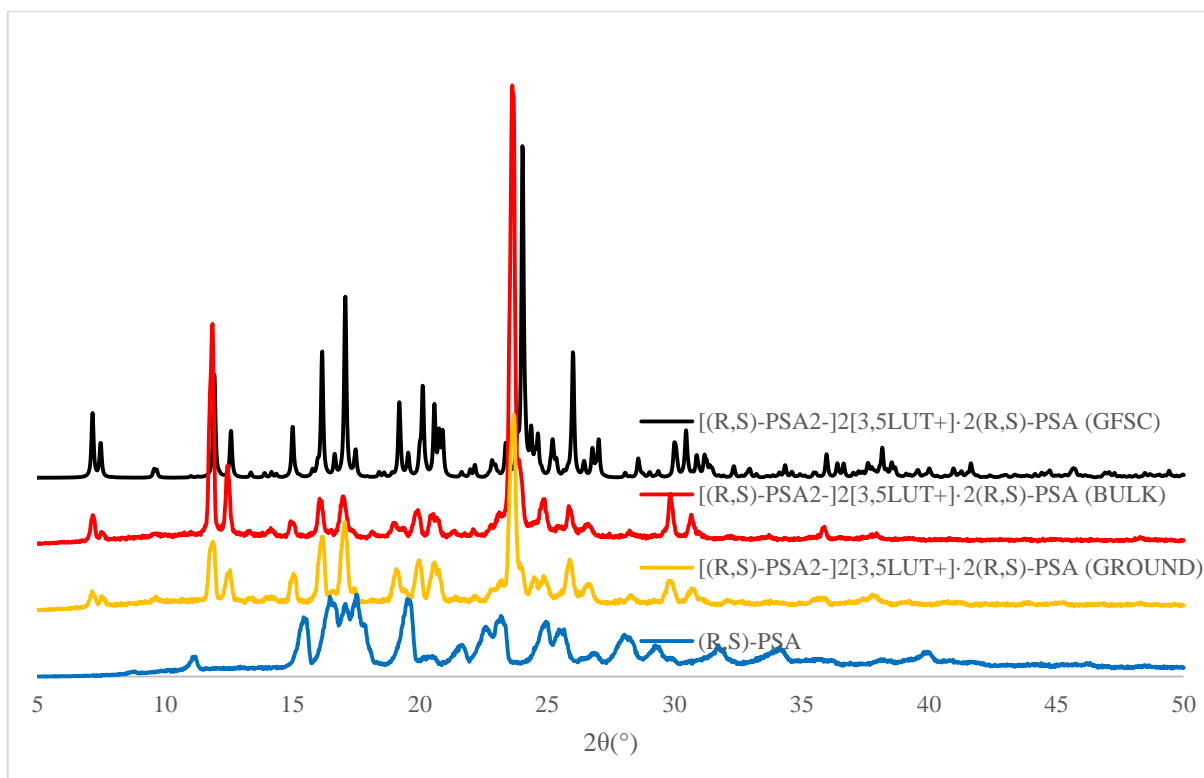


Figure S37 PXRD curve of $[(R,S)\text{-PSA}_2\text{-}]_2[3,5\text{LUT}^+] \cdot 2(R,S)\text{-PSA}$ and the starting material

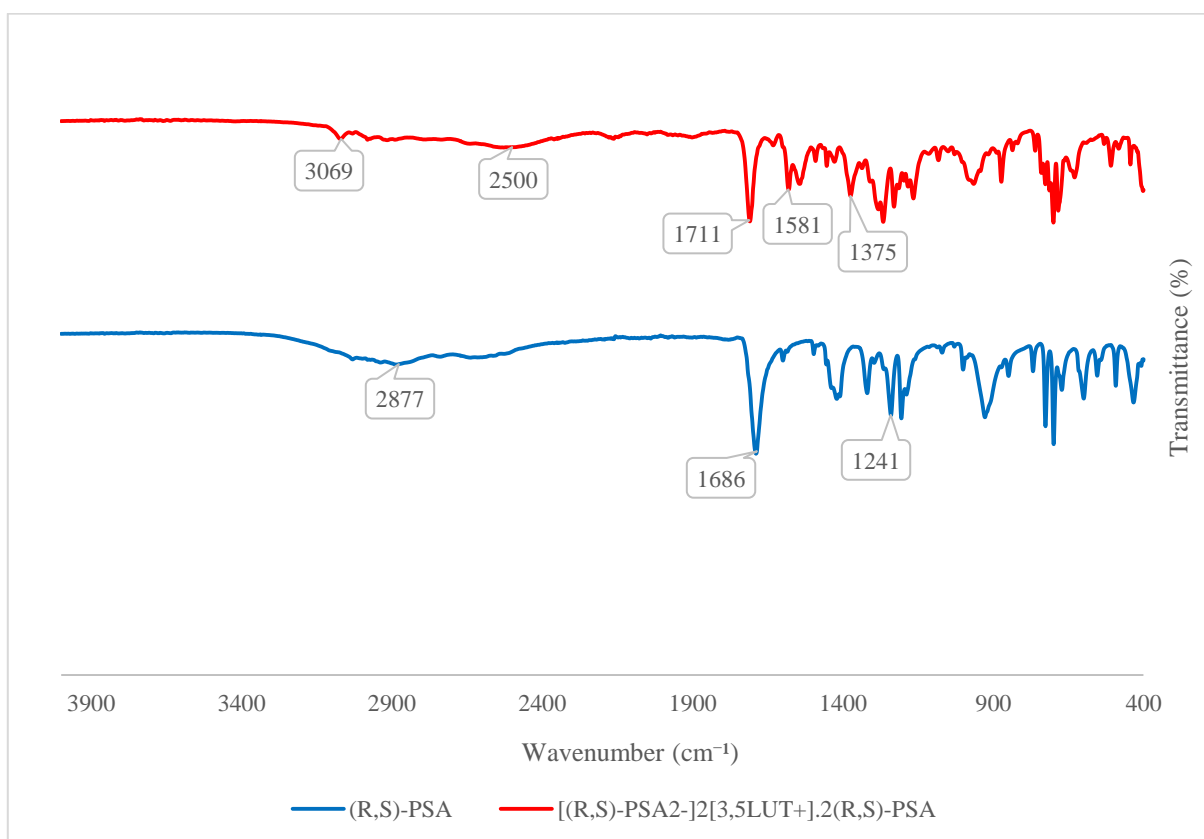


Figure S38 IR curve of $[(R,S)\text{-PSA}_2\text{-}]_2[3,5\text{LUT}^+] \cdot 2(R,S)\text{-PSA}$ and the starting material

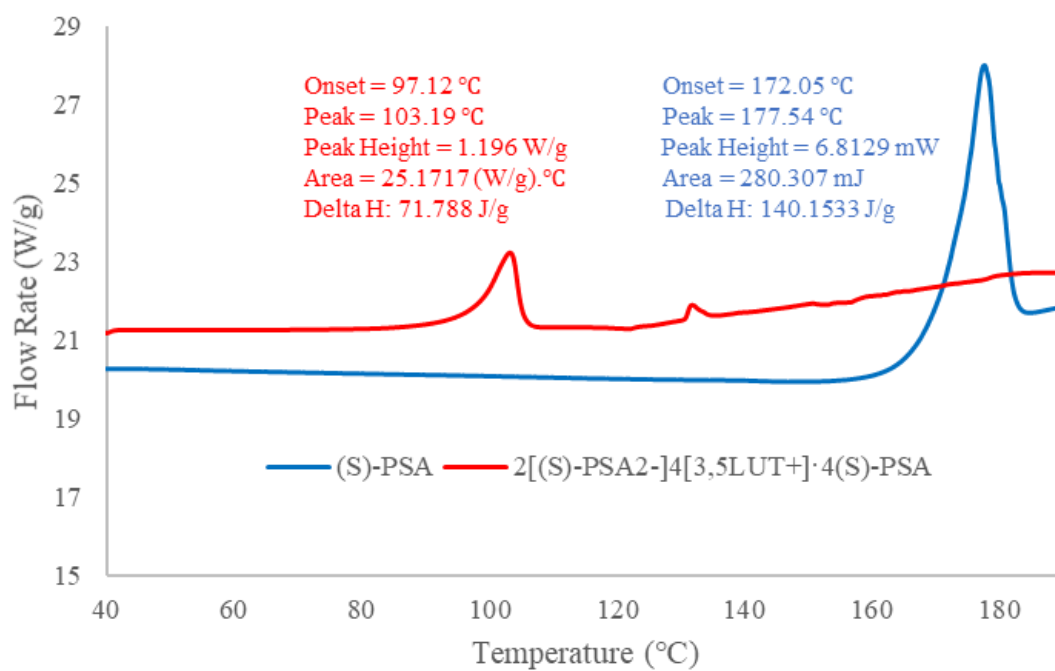


Figure S39 DSC curve of 2[(S)-PSA²⁻]₄[3,5LUT⁺]₄(S)-PSA and the starting material

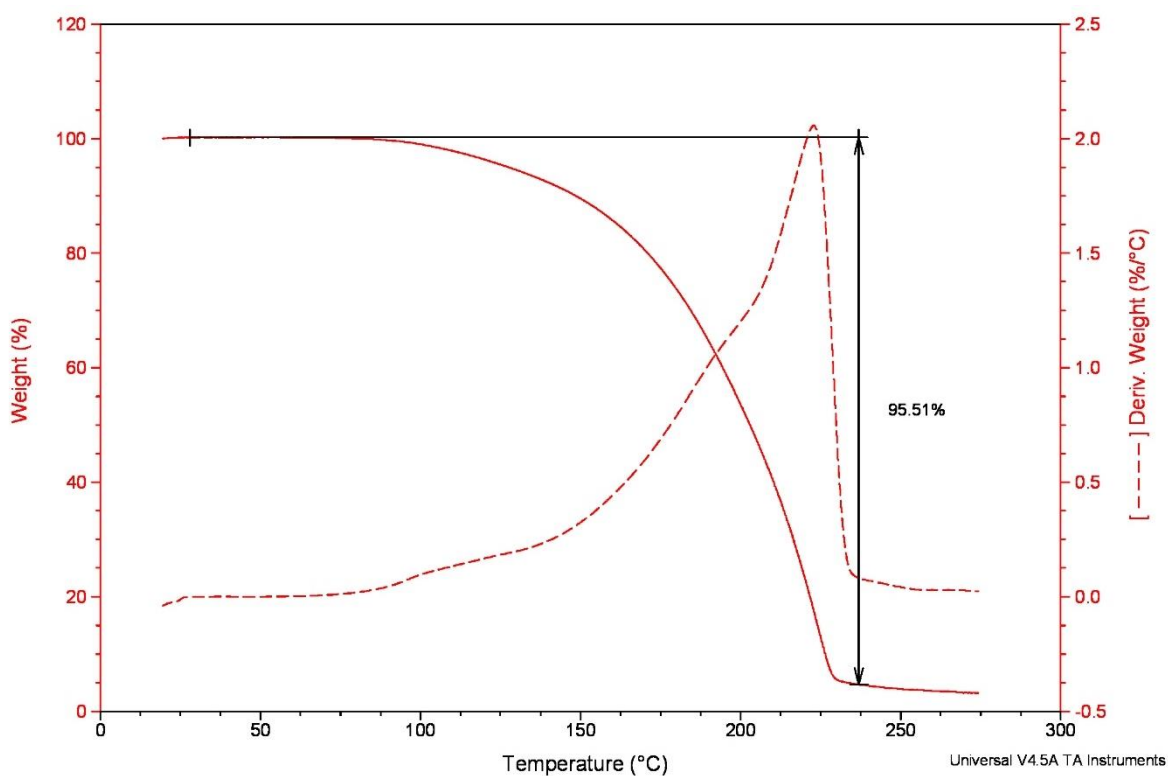


Figure S40 TG curve of 2[(S)-PSA²⁻]₄[3,5LUT⁺]₄(S)-PSA

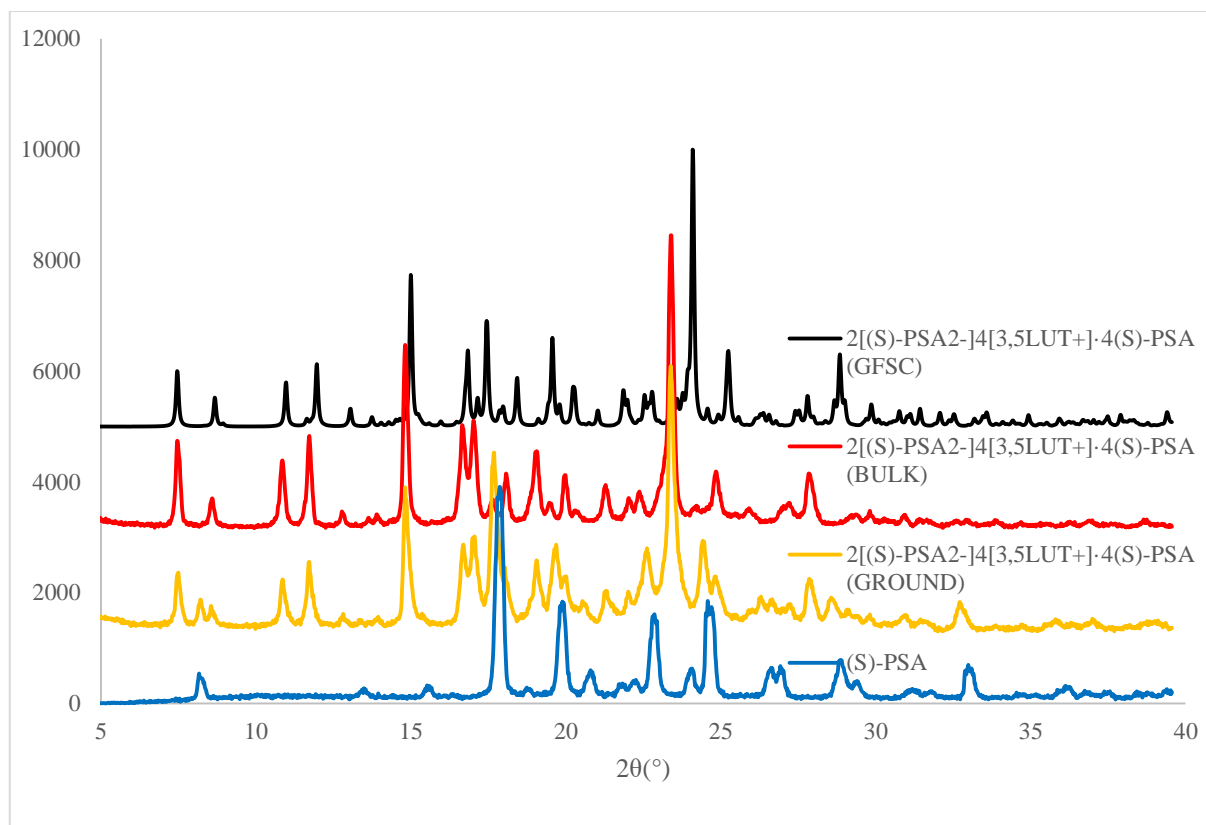


Figure S41 PXRD curve of $2[(S)\text{-PSA}^{2-}]_4[3,5\text{LUT}^+] \cdot 4(S)\text{-PSA}$ and the starting material

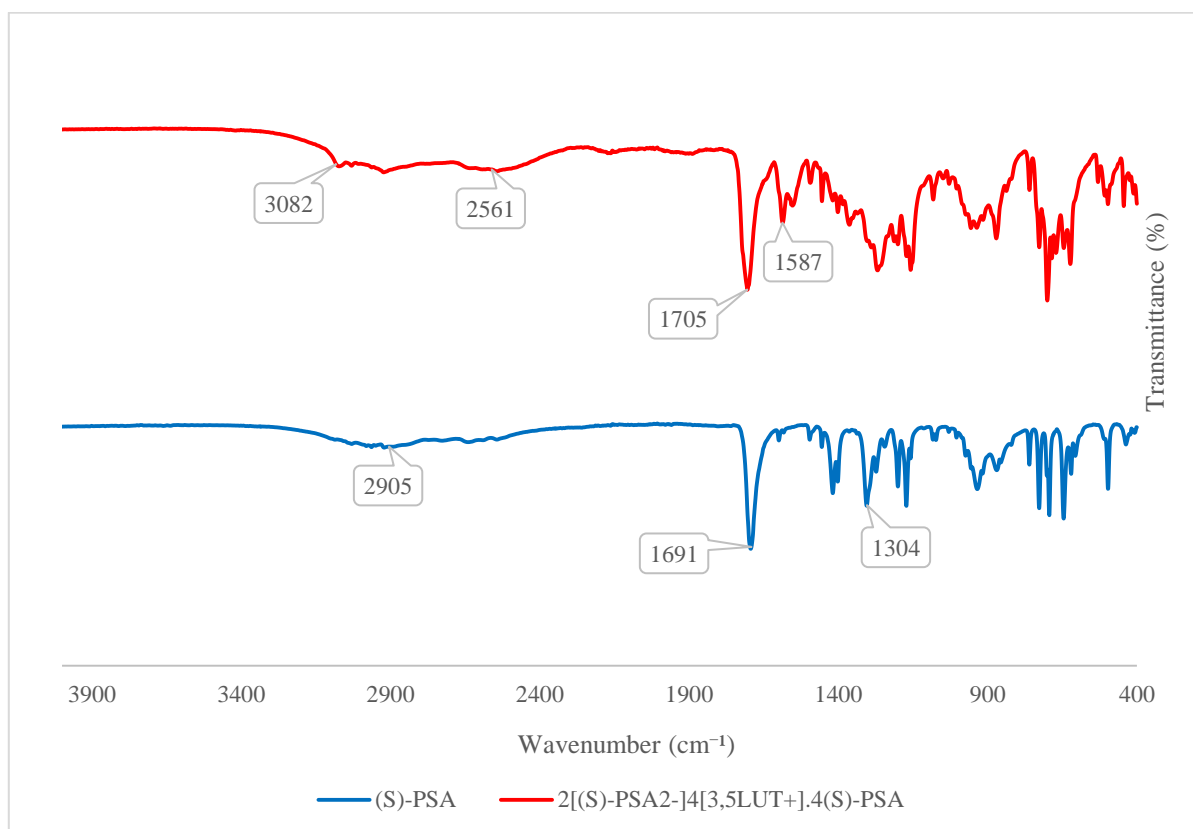


Figure S42 IR curve of $2[(S)\text{-PSA}^{2-}]_4[3,5\text{LUT}^+] \cdot 4(S)\text{-PSA}$ and the starting material

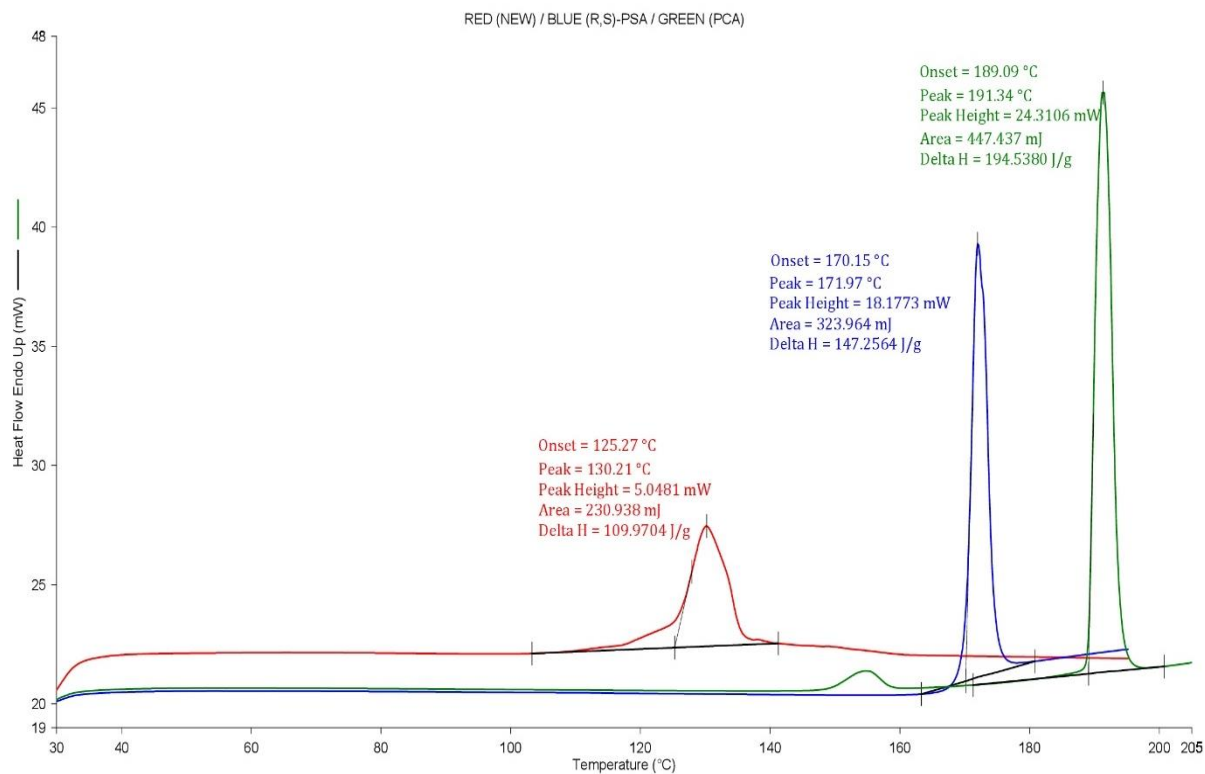


Figure S43 DSC curve of (R/S)-PSA·PCA and the starting materials

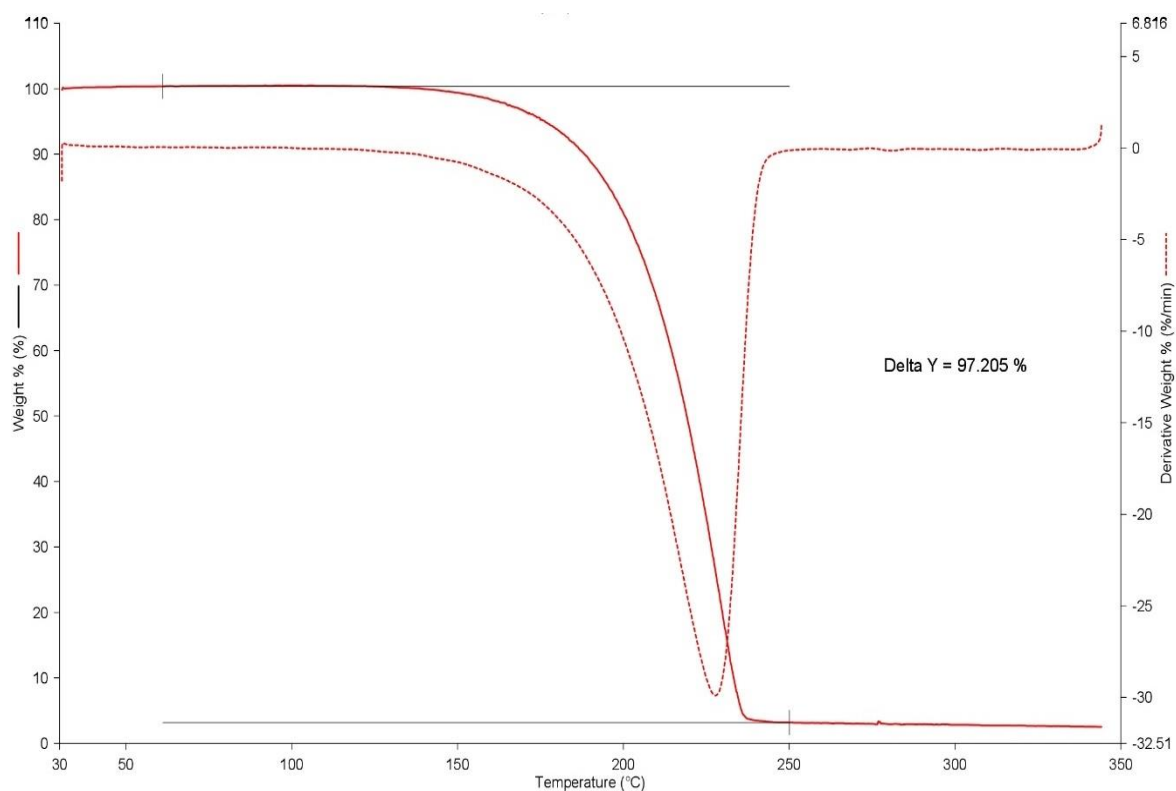


Figure S44 TG curve of (R/S)-PSA·PCA

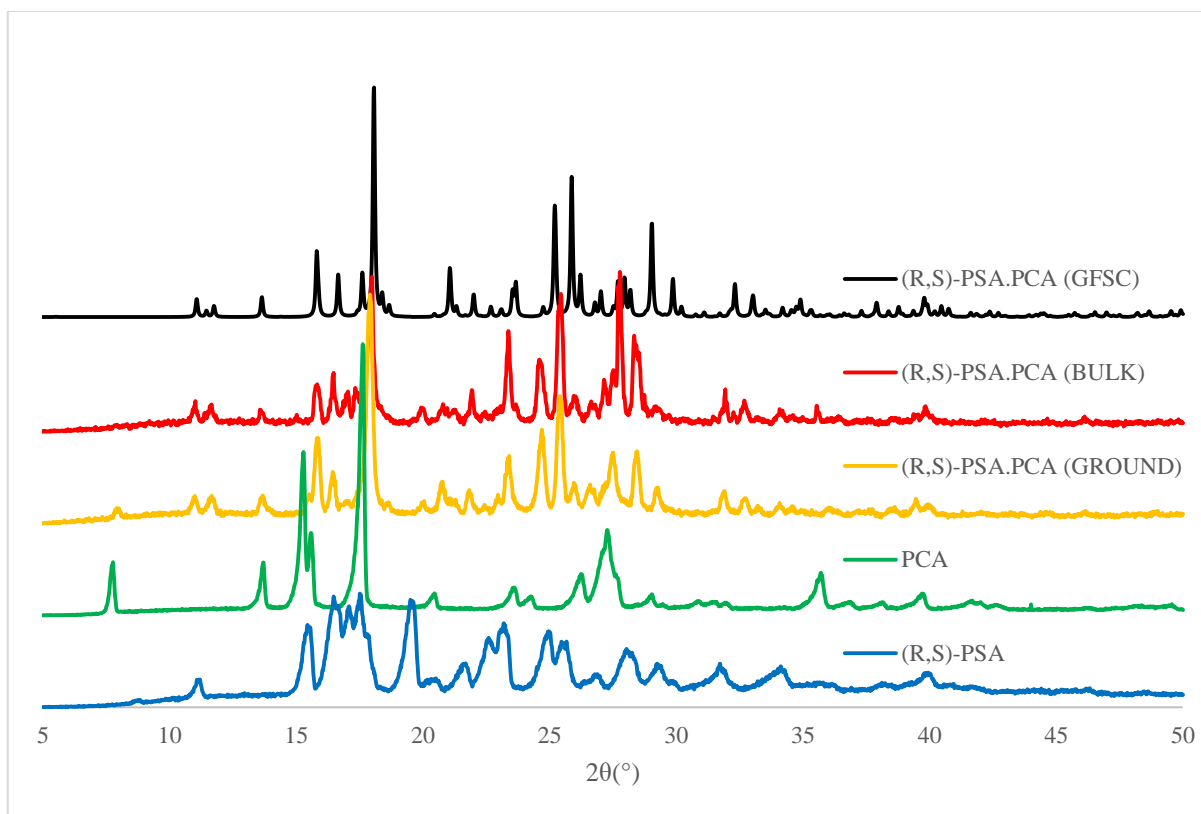


Figure S45 PXRD curve of (R/S)-PSA·PCA and the starting materials

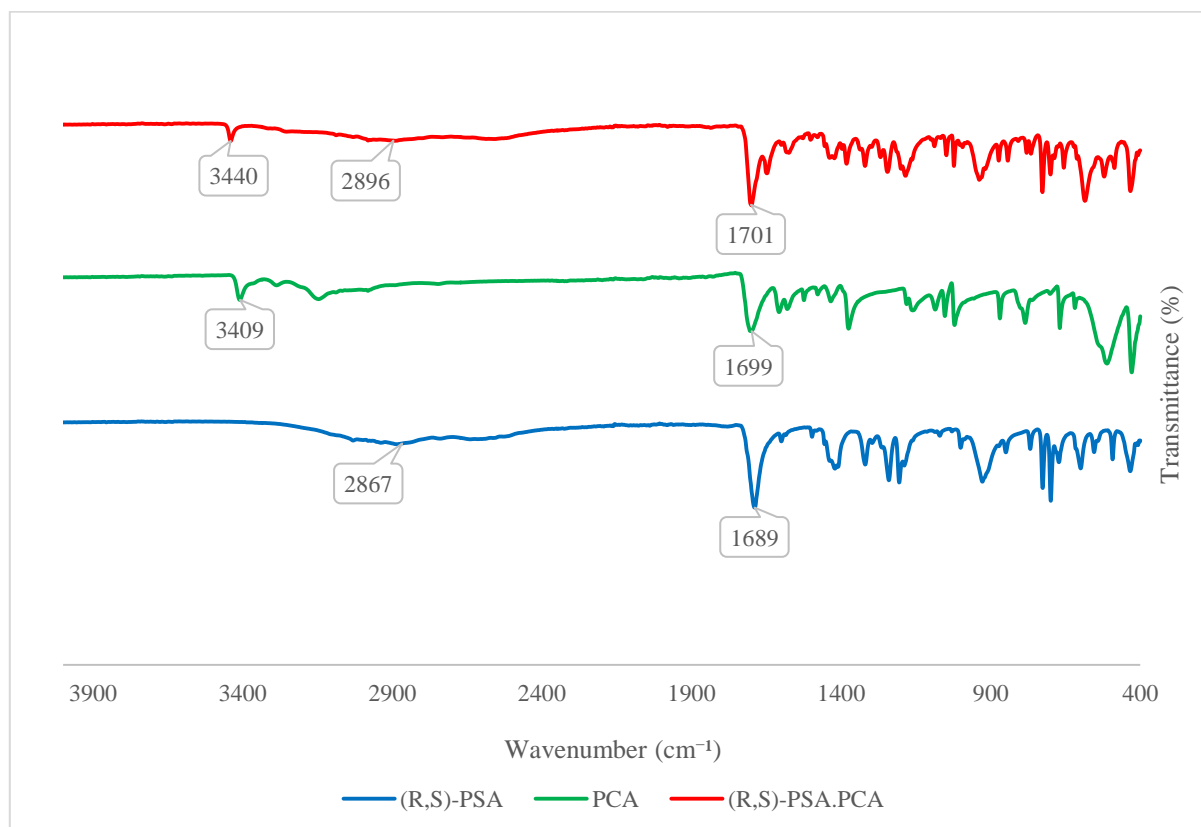


Figure S46 IR curve of (R/S)-PSA·PCA and the starting materials